Instituto Nacional de Astrofísica, Optica y Electrónica.

ANTIREFLECTIVE EMBEDDED MSM PHOTODETECTOR: AN ARCHITECTURAL OPTIMIZATION

By

Guillermo Fernando Camacho González

A dissertation submitted in partial satisfaction of the requirements for the degree of

Master in Sciences,
with the specialty in optics

Supervised by: Dr. J. Javier Sánchez-Mondragón
Dr. Pieter G. Kik
Dr. Ponciando Rodriguez Montero

Mayo 2015, TONANTZINTLA, PUEBLA

CONTENTS

TABLE OF FIGURES

TABLES

CHAPTER 1

1. INTRODUCTION

Photodetectors are essential elements in optoelectronics because they are the communication via between light and electronics. There are several kinds of photodetectors but nowadays the most used are semiconductor photodetectors due to its versatility when detecting light of specific wavelengths efficiently and with fast response velocity.

Most semiconductor photodetectors are fabricated with striped interdigitated electrodes over a semiconductor substrate (MSM photodetectors), in order that we have periodicity between metallic electrodes and semiconductor regions on top photodetector surface. These kind of photodetectors are widely used in communications due to its faster response compared to other photodetector structures[1,2,3] and they are a very good for UV detection[4,5]. Light is detected when it reaches the semiconductor region by creating charge carriers (holes and electrons) that are then transported to the electrodes due to an applied voltage difference[6]. Interdigitated electrodes are used to increase the active region area (semiconductor) while optimizing the electric fields between electrodes for carrier collection meaning high velocity response and sensitivity, but unfortunately it also provokes that certain amount of light get back reflected by the electrodes surfaces. Many methods to compensate this loss have been proposed, some examples are: using metallic gratings

[1] H. C. Lee and B. Van Zeghbroeck, " A novel high-speed silicon MSM photodetector operating at 830 nm wavelength," Electron Device Letters, IEEE, vol. 16, no. 5, pp. 175-177, 1995.
[2] J. B. Soole and H. Schumacher, "InGaAs metal-semiconductor-metal photodetectors for long wavelength optical communications," IEEE Journal of Quantum Electronics, vol. 27, no. 3, pp. 737-752, 1991.
[3] J. H. Kim, H. T. Griem, R. A. Friedman, E. Y. Chan and S. Ray, "KIM, Jae H., et al. High-performance back-illuminated InGaAs/InAlAs MSM photodetector with a record responsivity of 0.96 A/W," *IEEE Photonics Technology Letters,* vol. 4, no. 11, pp. 1241-1244, 1992.
[4] F. Omnès, E. Monroy, E. Muñoz and J.-L. Reverchon, "Wide bandgap UV photodetectors : A short review of devices and applications," *In Integrated Optoelectronic Devices 2007. International Society for Optics and Photonics,* vol. 6473, p. 6473E, 2007.
[5] A. Müller, G. Konstantinidis, M. Dragoman, D. Neculoiu, A. Dinescu, M. Androulidaki, M. Kayambaki, A. Stavrinidis, D. Vasilache, C. Buiculescu, I. Petrini, C. Anton, D. Dascalu and A. Kostopoulos, "Ultraviolet MSM photodetector based on GaN micromachining," *IEEE In Semiconductor Conference, 2008. CAS 2008. International,* vol. 1, pp. 91-94, 2008.
[6] R. D. L. IBM Corporation, "INTERDIGITATED SCHOTTKY BARRIER PHOTODETECTOR". United States of America Patent 4,772,931, 20 SEPTEMBER 1988.

on semiconductor to take advantage of the enhanced transmission effect[7,8,9], with periodically patterned electrodes resulting in plasmon-enhanced transmission or plasmonic-Brewster angle[10,11], resonant cavity enhanced phenomenon[12,13,14], using graphene layers as light absorbers[15,16], shaped electrodes that minimize the dark current[17], and finally a novel photodetector architecture that annihilate this back reflection has been proposed by Pieter G. Kik[18], which allows us to use the Total Internal Reflection by providing a tilt to the electrodes surfaces and embed them along with the photodetector surface into a transparent medium.

The central objective of this thesis is to make a thorough numerical study of the transmission and reflection of visible light through the novel photodetector design proposed by Pieter G. Kik in ref. [10]. This numerical study will allow us to improve the photodetector architecture by finding the best dimensions and characteristics to have a high transmission. The high transmission will increase the photodetector sensitivity and the new dimensions will let us improve the response speed.

The aim of the thesis is to promote the fabrication and use of the improved photodetector. In addition I wish to familiarize the lector with the concepts of photodetectors, reflection and transmission of waves and anti-reflection layers. After a good assimilation of these concepts it will be easier to understand the interaction of light with photodetectors.

---

[7] G. F. Camacho-Gonzalez, O. Olmos-Lopez, J. Sumaya-Martinez and M. Mayorga-Rojas, "Enhanced transmission through metallic subwavelength slits," *In Eighth Symposium Optics in Industry. Internation Society of Optics and Photonics,* vol. 8287, p. 82870T, 2011.

[8] X. Hu, M. Li, Z. Ye, W. Y. Leung, K.-M. Ho and S.-Y. Lin, "Design of midinfrared photodetectors enhanced by resonant cavities with subwavelength metallic gratings," *Applied Physics Letters,* vol. 93, 2008.

[9] R. A. Pala, J. S. Liu, E. S. Barnard, D. Askarov, E. C. Garnett, S. Fan and M. L. Brongersma, "Optimization of non-periodic plasmonic light-trapping layers for thin-film solar cells," *NATURE COMMUNICATIONS,* vol. 4, 2013.

[10] C.-C. Chang, Y. D. Sharma, Y.-S. Kim, J. A. Bur, R. V. Shenoi, S. Krishna, D. Huang and S.-Y. Lin, "A Surface Plasmon Enhanced Infrared Photodetector Based on InAs Quantum Dots," *NANO Letters,* vol. 10, no. 5, p. 1704–1709, 2010.

[11] S. Collin, F. Pardo and P. Jean-Luc, "Resonant-cavity-enhanced subwavelength metal–semiconductor–metal photodetector," *Applied Physics Letters,* vol. 83, 2003.

[12] K. Kishino, M. S. Ünlü, J.-I. Chyi, J. Reed, L. Arsenault and H. Morkoç, "Resonant Cavity-Enhanced (RCE) Photodetectors," *IEEE Journal of Quantum Electronics,* vol. 27, no. 8, pp. 2025-2034, 1991.

[13] J. B. Héroux, Y. X. and W. I. Wang, "GaInNAs resonant-cavity-enhanced photodetector operating at 1.3 mm," Applied Physics Letters, vol. 75, no. 18, pp. 2716-2718, 1999.

[14] A. Alù, G. D'Aguanno, N. Mattiucci and M. J. Bloemer, "Plasmonic Brewster Angle: Broadband Extraordinary Transmission through Optical Gratings," *Physical Review Letters,* vol. 106, no. 12, p. 123902, 2011.

[15] F. Xia, T. Mueller, Y. M. Lin, A. Valdes-Garcia and P. Avouris, "Ultrafast graphene photodetector," *Nature nanotechnology,* vol. 4, no. 12, pp. 839-843, 2009.

[16] T. Mueller, F. Xia and P. Avouris, "Graphene photodetectors for high-speed optical communications," *Nature Photonics,* vol. 4, no. 5, pp. 297-301, 2010.

[17] Z. Song, P. Wang, L. Guo, Y. Yang and Q. & Tang, "Asymmetric semicircular and triangular electrode structures to increase photo-to-dark-current ratio in MgZnO metal semiconductor metal photodetectors," *Japanese Journal of Applied Physics,* vol. 54, no. 5, p. 052201, 2015.

[18] P. G. Kik, "Catoptric electrodes: transparent metal electrodes using shaped surfaces," *Optics Letters,* vol. 39, no. 17, 1 September 2014.

1.1. EMBEDDED PHOTODETECTOR

The photodetector to study consists in a semiconductor substrate covered with an Antireflection Layer (ARL) followed by the interdigitated silver electrodes on top, all embedded in a transparent medium which is also covered by an anti-reflection layer as it is shown in Figure 1-1.

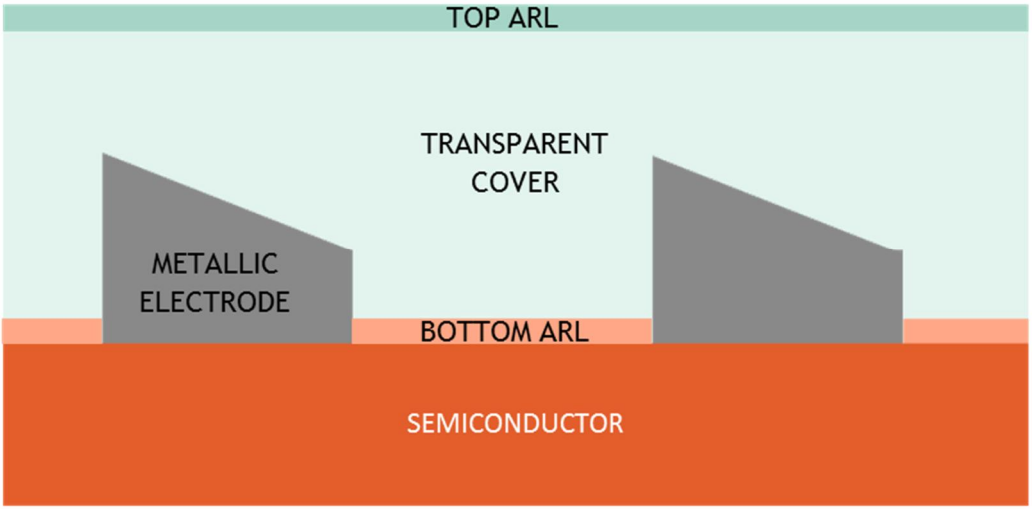

FIGURE 1.1 TRANSVERSAL VIEW OF THE EMBEDDED PHOTODETECTOR DESIGN CONSISTING IN A SEMICONDUCTOR(DARK ORANGE) COVERED WITH AN ARL(LIGHT ORANGE) AND A COUPLE TILTED ELECTRODES(GRAY), ALL EMBEDDED IN TRANSPARENT MEDIUM(TRANSPARENT BLUE) WITH ITS RESPECTIVE ARL(BLUE FRINGE).

For a detailed study, the photodetector was divided in basic simpler regions and they were studied separately. If we follow the path of the incoming light onto the photodetector's surface, we find that light interactions are in the following order:

a) First it finds a dielectric surface in which we analyze the wave equations resulting from Maxwell equations, then we apply the pertinent boundary conditions and obtain the reflection and transmission of light expressions. When we plot we notice that there is always a fraction of light reflected when it changes of medium and that's why we need antireflection layers.

b) Light strikes to a second surface; if the distance between this and the last surface fulfill certain conditions, then we will have an ARL. Theoretically it was found that the refractive index for the inner medium has to the square root of the surrounding media ($n_{ARL} = \sqrt{n_i n_t}$, where n_{ARL} , n_i and n_t are the ARL, incident and transmitted refractive indexes respectively). By numerical simulation of the transmission of light through both boundaries, we find that the distance between boundaries has to be an integer multiple of the

wavelength over four times ($d = \lambda/4n_{ARL}$, where d is the distance between boundaries and λ the light wavelength).

c) Some light will bounce in the metallic tilted electrode. By numerical analysis it is found that conductive media absorb light, but also has a high reflectance. We will find the metal with higher reflection for visible light.

d) Bounced light will be back reflected due to the Total Internal Reflection (TIR). With a geometrical analysis we will find the best thickness for the transparent medium and the necessary condition for TIR.

e) At the end, light achieves the semiconductor, which is a lossy medium, so we find the ideal ARL numerically.

f) Finally, we present CST STUDIO SUITE® simulation results of the reflected light by the photodetector and their interpretation.

1.2. DISTRIBUTION OF THE THESIS

With the purpose of a better understanding of the lector, this thesis is distributed in the next order:

1. Chapter two contains all the theoretical background used in the photodetectors study and is divided in the next topics:
    a. **Photodetectors**, its main features and how semiconductor photodetectors work. It is important because this will help to understand how the improvements will work in light detection and the advantages of the proposed design.

    b. **Wave nature of light**, an explanation and its behavior when it travels from one medium to another. Here we deduce the wave equation from Maxwell´s equations and apply boundary conditions to obtain the Reflection and transmission through a boundary.

    c. **Total internal Reflection (TIR)**, using theoretical considerations it is easy to demonstrate the necessary conditions for TIR to occur.

    d. **Reflection in Metals**, the optical properties of metals and its implications.

    e. **Anti- Reflection Layers (ARL)**, we obtain transmission and reflection equations for two parallel boundaries and show the necessary conditions to have an ARL.

2. Chapter three is a detailed description of the **photodetector characteristics selection process**, so it contains calculations and numerical simulations that let us get the better behavior of each part if the photodetector. In this chapter the lector will see the theoretical background applied to the problem.

3. Chapter four presents reflection simulation **results** for different photodetector configurations and its corresponding interpretations. We used a software called CST STUDIO SUITE®, which is used for simulate a wide range of electromagnetic design tasks.

4. Chapter five contains the conclusions, here we highlight the advantages of the photodetector design, its implications and possibilities.

With this we conclude the thesis content wishing the lector to have a clear understanding of it.

CHAPTER 2

2. THEORETICAL FRAMEWORK

The scope of this chapter is to introduce the reader into the necessary concepts and theory to understand the problem studied in this thesis. From de definition of a photo detector until the behavior of light interacting with each one of its components, this chapter will provide a thorough understanding of an MSM photodetector performance.

2.1. PHOTODETECTORS

The electromagnetic radiation is assorted by frequency or wavelength in what we call "electromagnetic spectrum", which extends from the very short wavelengths of gamma rays (typically < 10^{-12} m) to radio waves which can be thousands of meters in wavelength. The region of the spectrum encompassing the ultraviolet, visible an infrared radiation is known as the optical region and extends from 0.01 to 1,000 micrometers of wavelength (see Figure 2-1). Radiation detectors suitable to operate in this region are called photodetectors.

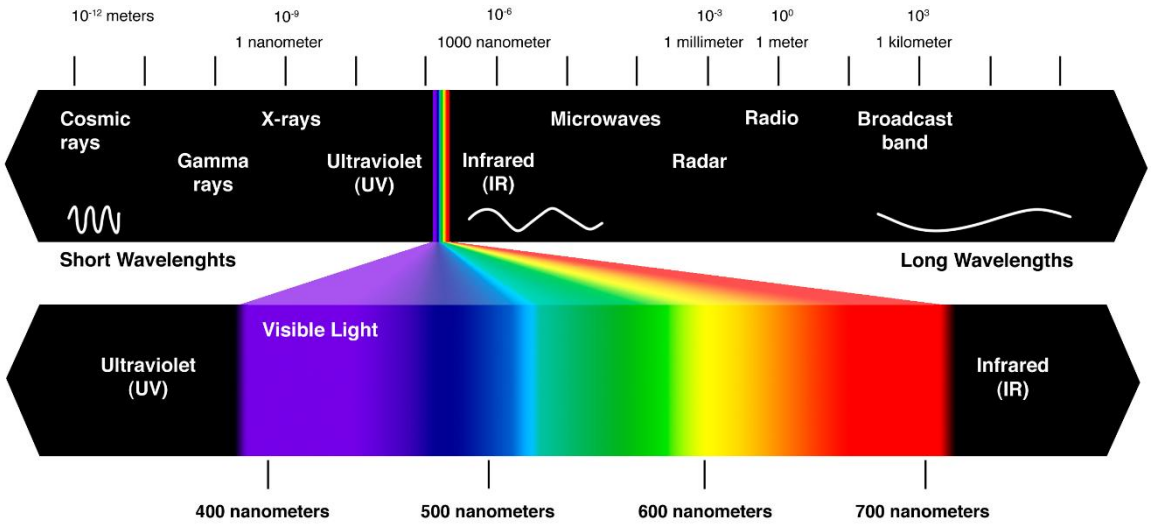

FIGURE 2.1 OPTICAL REGION OF THE ELECTROMAGNETIC SPECTRUM IN WAVELENGTHS (TAKEN FROM REF. 19)[19]

[19]"LENA Lighting," 2010. [Online]. Available: http://www.lenalighting.pl/en/knowledge/spectrum-of-visible-radiation/.

The majority photodetectors can be classified into two main branches: thermal photodetectors and photon detectors. The first branch senses light indirectly, by detecting temperature changes produced by light absorption, and the second branch work through the excitation of electrons produced by the photons absorption (photons are the light quanta and their energy is inversely dependent of the wavelength $E = hc/\lambda$ where h is planck's constant an c the speed of light in vacuum). For the purpose of this thesis we are going to ignore thermal photodetectors because their structure differs a lot from the studied here.

Within photon detectors there are two distinct categories according to the detection method:

- **Photoemissive device**: These detectors take advantage of the photoelectric effect, where the electrons are excited and emitted from a photosensitive electrode after absorbing light photons. They totally scape from the electrode and are then collected for detection.

- **Solid State Sensors**: Photons cause a change in the electronic energy distribution within the material in what we call "Internal photoelectric effect", because electrons are not completely extracted from the material. For example, when light strikes a photoconductor, the number of free electrons varies and an associated change in conductivity is provoked and measured.

Semiconductors are the ideal materials for internal photoelectric effect detectors because of the high mobility of charge carriers (speed of response), the low dark current (sensitivity) and the predominance of electron-hole generation compared to phonon generation or single carrier excitation (high efficiency).

2.1.1. SOLID STATE PHOTODETECTORS

Solid State sensors are the ones that can take advantage of the embedded tilted electrodes design because the surface of most of them consist in a semiconductor window between metallic electrodes and in many cases, interdigitated electrodes.

A solid state photodetector operates thank to the electrical properties of semiconductors, which can behave either as a conductor or as an insulator. Current conduction in a semiconductor occurs through the collective movement of free electrons (negative charge) and holes (positive charge), known as "charge carriers". Adding impurity atoms to a semiconducting material, known as "doping", greatly increases the number of charge carriers within it. When a doped semiconductor contains mostly free holes it is called "p-type", and when it contains mostly free electrons it is known as "n-type". The semiconductor materials used in photodetectors are doped under precise conditions to control the concentration and regions of p- and n-type dopants.

Light detection consists in the basic steps listed below:

1. ***Create carriers***: Initially they are combined within the semiconductor atoms (valence electrons) but they can be separated by a photon if it has enough energy.

2. ***Transport carriers***: Once carriers are created, they can be driven to the electrodes by applying a voltage difference between them.

3. ***Measure voltage or current variations***: when the carriers are transported to the electrodes, they contribute to current and voltage variations that can be measured revealing the interaction of light with the semiconductor.

The energy required to excite valence electrons is represented in Energy band diagrams like the one shown in Figure 2-2, where the lower energy region filled with blue dots represent the "valence band" originally with each blue dot being a hole-electron pair, the upper band is where electrons move free and it is called "conduction band" and between these bands we have the "band gap", where the possibility of find electrons is almost cero. Initially in a regular semiconductor there are no electrons in the conduction band so they behave as insulators, but light with energy equal or greater to the band gap strikes the material, then electrons jump from the valence to de conduction band so the semiconductor behaves as a conductive material.

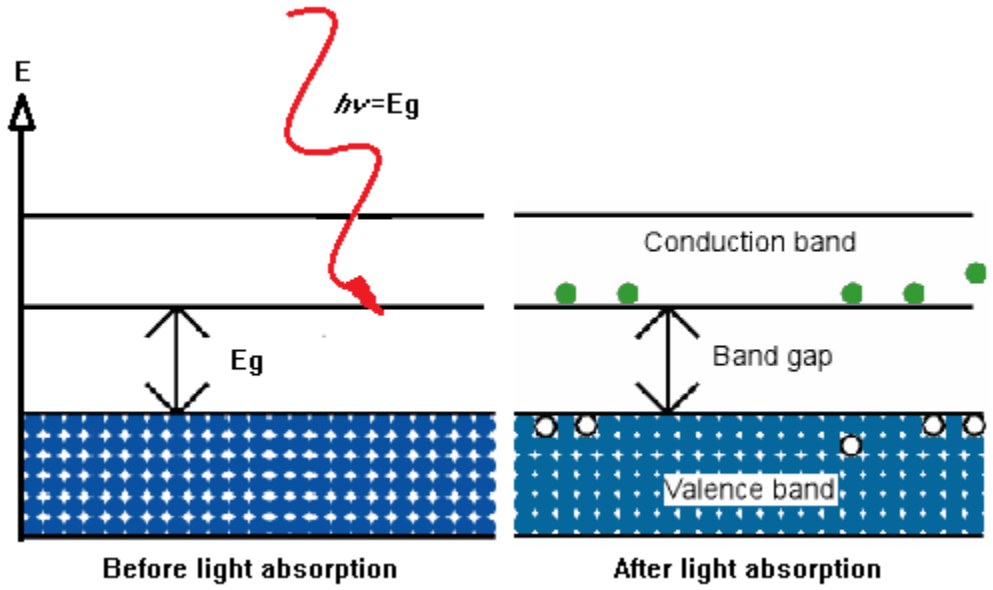

FIGURE 2.2 INTERNAL PHOTOELECTRIC EFFECT IN ENERGY BANDS DIAGRAM, WHERE Y AXIS IS THE ENERGY AND THE X AXIS REPRESENT THE MATERIAL EXTENSION. BLUE DOTS REPRESENT COMBINED ELECTRON-HOLES, GREEN DOTS ARE ELECTRONS AND WHITE CIRCLES ARE HOLES. (ADAPTED FROM REF. 20).[20]

Although there are many kinds of solid state sensors (p-n junction, p-i-n junction, Schottky junction, metal-semiconductor-metal, avalanche… etc. (see ref. [1])) with very varied designs, we

[20] D. J. Wagner, "Glossary for Semiconductors," Rensselaer Polytechnic Institute, 2004. [Online]. Available: http://www.rpi.edu/dept/phys/ScIT/InformationProcessing/semicond/sc_glossary/scglossary.htm.

are going to focus in the metal-semiconductor-metal (MSM) photodetectors, which design corresponds to interdigitated electrodes like those shown in Figure 2.3.

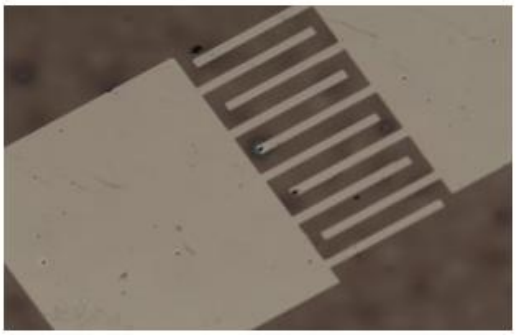

FIGURE 2.3 TOP VIEW OF INTERDIGITATED ELECTRODES. (TAKEN FROM REF. 21)[21]

2.1.2. MSM PHOTODETECTOR PROPERTIES

MSM photodetector is the combination of two metal-semiconductor junctions also called "Schottky junctions". To study any junction with band diagrams, it is necessary to define the "Fermi Level". The Fermi level is the total chemical potential for electrons (or electrochemical potential for electrons), it means, the thermodynamic work required to add one electron to the body. In a band structure picture, the Fermi level can be considered to be a hypothetical energy level of an electron, such that at thermodynamic equilibrium this energy level would have a 50% probability of being occupied at any given time, if it does not lie in the forbidden gap. The Fermi level does not necessarily correspond to an actual energy level, for example in an insulator the Fermi level lies in the band gap (dotted line in Figure 2.4). Now, when we bring together a semiconductor with a metal, the free electrons on the semiconductor induce a positive charge at the metal and when they make contact, free electrons are attracted to the metal and Fermi Levels coincide in the junction bending the band gap as it is shown in Figure 2.4. If there are carriers created at mid semiconductor, they may take a long time for them to be collected.

[21] "Indian Nanoelectronics User's Programme," INUP IISC BANGALORE, 2010. [Online]. Available: http://www.nano.iisc.ernet.in/inup/ghusoonali.html.

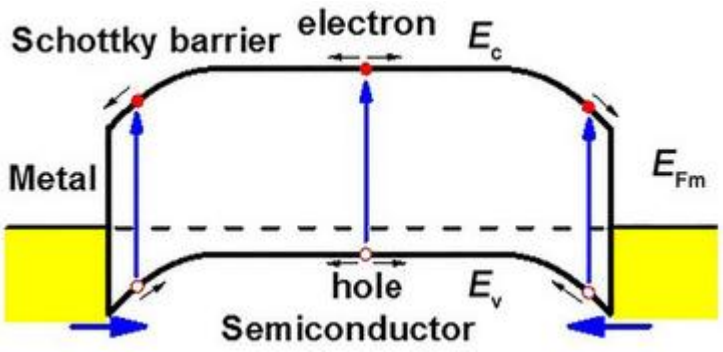

FIGURE 2.4 BAND DIAGRAM OF THE METAL-SEMICONDUCTOR-METAL JUNCTION AT THERMAL EQUILIBRIUM, E_C IS CONDUCTION ENEREGY AN E_V THE VALENCE ENERGY.(ADAPTED FROM REF. 22)[22]

Carriers' collection is improved by applying a Voltage V_{DS} between the metals, this provokes a slide like bending of the band gap, and thus carriers created in any part of the semiconductor will slide to the corresponding electrode (holes to the cathode and electrons to the anode) as shown in Figure 2-5.

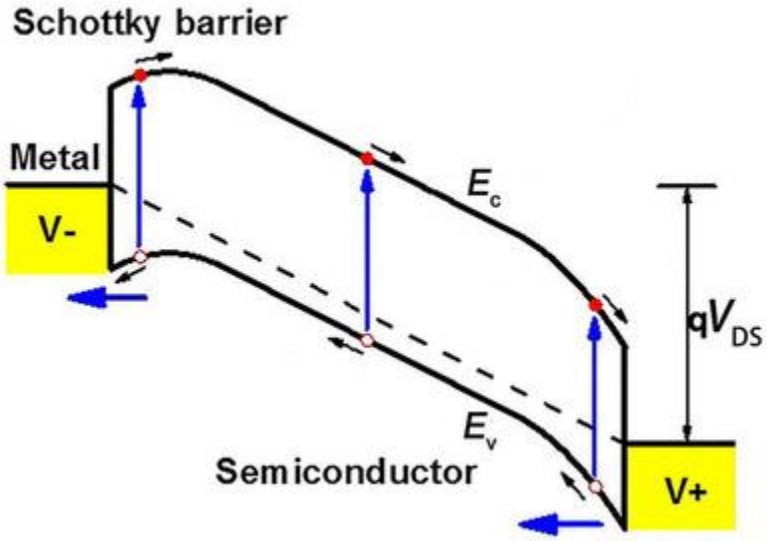

FIGURE 2.5 BAND DIAGRAM OF A METAL-SEMICONDUCTOR-METAL JUNCTION AFTER AN APPLIED VOLTAGE V_{DS}. (ADAPTED FROM REF. 22)

MSM photodetectors have been the focus of much recent research. The monolithic design, integration feasibility with standard VLSI (Very Large-Scale Integration) circuitry, high speed

[22] Y. Cao, K. Cai, P. Hu, L. Zhao, T. Yan, W. Luo, X. Zhang, X. Wu, K. Wang and H. Zheng, "Strong enhancement of photoresponsivity with shrinking the electrodes spacing in few layer GaSe photodetectors," *scientific reports,* vol. 5, no. 8130, 2015.

performance, and applicability to 2-D array layouts make them a good candidate for optical interconnect components. In many optical interconnect schemes, the combination of low optical power emission from optical sources, low cost and low efficiency optical guiding or focusing systems and realistic alignment limitations often result in a low optical signal level reaching the photodetector. So the photodetector architecture presented in this thesis has the purpose of take advantage of all the incident radiation to overcome the low optical signal.

2.2.WAVE NATURE OF LIGHT

In 1845 the master experimentalist Michael Faraday (1791-1867) established an interrelationship between electro-magnetism and light when he found that the polarization direction of a beam could be altered by a strong magnetic field applied to the medium. James Clerk Maxwell (1831-1879) brilliantly summarized and extended all the empirical knowledge on the subject in a single set of mathematical equations. Beginning with this remarkably succinct and beautifully symmetrical synthesis, he was able to show, purely theoretically, that the electromagnetic field could propagate as a transverse wave in the ether.[23]

2.2.1. MAXWELL'S EQUATIONS AND THE WAVE EQUATION

To find the wave equation that describes the light behavior we can start from writing the four equations that describe every electro-magnetic effect, these are known as Maxwell's equations and in their differential form they are

$$\nabla \cdot \vec{E} = \frac{\rho}{\epsilon} \tag{2.1}$$

$$\nabla \cdot \vec{B} = 0 \tag{2.2}$$

$$\nabla \times \vec{E} = -\frac{\partial \vec{B}}{\partial t} \tag{2.3}$$

$$\nabla \times \vec{B} = \mu\sigma\vec{E} + \mu\epsilon\frac{\partial \vec{E}}{\partial t} \tag{2.4}$$

Where $\vec{E}$ is the Electric field vector, $\vec{B}$ is the Magnetic field vector, ρ is the free charge density, ϵ the electric permittivity, μ the magnetic permeability and σ the material conductivity. Taking the curl of equation 2.4, we obtain

$$\nabla \times (\nabla \times \overrightarrow{B}) = \mu\sigma\nabla \times \vec{E} + \mu\epsilon\frac{\partial \nabla \times \vec{E}}{\partial t} \tag{2.5}$$

[23] E. Hecht, Optics, San Francisc, CA: Adison Wesley, 2002.

where, since $\vec{E}$ is assumed to be a well-behaved function, the space and time derivatives can be interchanged. Equation 2.3 can be substituted to obtain the needed second derivative with respect to time:

$$\nabla \times (\nabla \times \overrightarrow{B}) = -\mu\sigma \frac{\partial \vec{B}}{\partial t} - \mu\epsilon \frac{\partial^2 \vec{B}}{\partial t^2} \quad 2.6$$

The vector triple product can be simplified by making use of the operator identity

$$\nabla \times \left(\nabla \times \vec{B}\right) = \nabla\left(\nabla \cdot \vec{B}\right) - \nabla^2 \vec{B} \quad 2.7$$

Since the divergence of $\vec{B}$ is zero, equation 2.4 becomes

$$\nabla^2 \vec{B} - \mu\sigma \frac{\partial \vec{B}}{\partial t} - \mu\epsilon \frac{\partial^2 \vec{B}}{\partial t^2} = 0 \quad 2.8$$

Similarly, for uncharged medium (ρ = 0), we obtain an identical equation for $\vec{E}$

$$\nabla^2 \vec{E} - \mu\sigma \frac{\partial \vec{E}}{\partial t} - \mu\epsilon \frac{\partial^2 \vec{E}}{\partial t^2} = 0 \quad 2.9$$

Equations 2.8 and 2.9 are known as the equations of telegraphy and for non-conducting media the conductivity becomes zero (σ = 0), and these equations become

$$\nabla^2 \vec{B} - \mu\epsilon \frac{\partial^2 \vec{B}}{\partial t^2} = 0 \quad 2.10$$

$$\nabla^2 \vec{E} - \mu\epsilon \frac{\partial^2 \vec{E}}{\partial t^2} = 0 \quad 2.11$$

which are the so called “wave equations” and describes the light behavior. Where $\mu\epsilon = 1/c^2$ being *c* the speed of the light in vacuum.

When we solve this equations for the interaction of light with matter we have to use the named ”Boundary Conditions”, which say that the tangential component of the Electric and Magnetic fields are continuous in both sides of a boundary. In a surface in the (x,y) at z=0 it means

$$\vec{H}_y(x, z^- = 0) = \vec{H}_y(x, z^+ = 0)$$
$$\vec{E}_x(x, z^- = 0) = \vec{E}_x(x, z^+ = 0) \quad 2.12$$

2.2.2. FRESNEL REFLECTION AND TRANSMISSION COEFFICIENTS

Applying the boundary conditions to a simple plane wave incident on a single planar interface leads to the familiar Fresnel reflection and transmission coefficients. We only briefly mention the results.

An arbitrarily polarized plane wave $\overrightarrow{E_1}e^{\vec{k}_1\cdot\vec{r}-i\omega t}$ can always be written as the superposition of two orthogonally polarized plane waves. It is convenient to choose these polarizations parallel or perpendicular to the plane of incidence defined by the k-vector of the plane wave and the surface normal n of the plane interface

$$\overrightarrow{E_1} = \overrightarrow{E_1^s} + \overrightarrow{E_1^p} \qquad 2.13$$

E_1^S is parallel to the interface (also called TE polarization) while E_1^p is perpendicular to the wave vector k and $E_1^{(s)}$ (or TM polarization). The superscripts *s* and *p* stand for the German words "senkrecht" (perpendicular) and "parallel" (parallel), respectively, in reference to the plane of incidence [24]. Upon reflection or transmission at the interface, the polarizations *s* and p are conserved.

In Figure 2.6, ϵ_1 and ϵ_2 denote the dielectric constants of the medium of incidence and the medium of transmittance, respectively. The same designation applies to the magnetic permeability μ. Similarly, we distinguish between incident and transmitted wave vectors $\overrightarrow{k_1}$ and $\overrightarrow{k_2}$. Using the coordinate system shown in Figure 2.6, it follows from the boundary conditions that

$$\overrightarrow{k_1} = (k_x, k_y, k_{z1}), \quad |\overrightarrow{k_1}| = \frac{\omega}{c}\sqrt{\epsilon_1\mu_1} \qquad 2.14$$

$$\overrightarrow{k_2} = (k_x, k_y, k_{z2}), \quad |\overrightarrow{k_2}| = \frac{\omega}{c}\sqrt{\epsilon_2\mu_2} \qquad 2.15$$

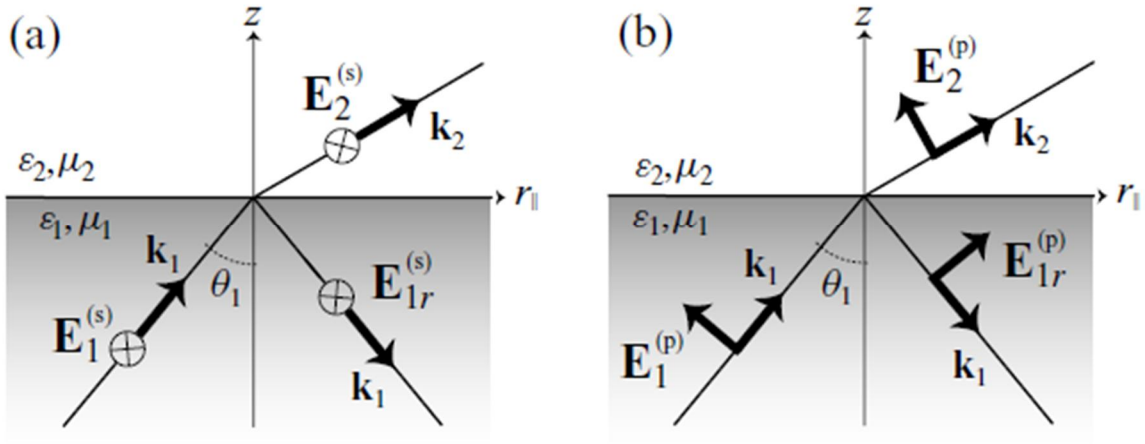

FIGURE 2.6 REFLECTION AND REFRACTION OF A PLANE WAVE AT A PLANE INTERFACE. (A) S-POLARIZATION, AND (B) P-POLARIZATION. (TAKEN FROM REF. 24)

[24] L. Novotny and B. Hecht, Principlel of Nano-Optics, New York: Cambridge University Press, 2006.

We may see the transverse components of the wave vector $(k_x\ , k_y)$ are conserved in space and the *z* component magnitude of the wave vectors are given by

$$k_{z1} = \sqrt{k_1^2 - \left(k_x^2 + k_y^2\right)}, \qquad k_{z2} = \sqrt{k_2^2 - \left(k_x^2 + k_y^2\right)} \tag{2.16}$$

The wave vector component transverse to the surface $k_{||} = \sqrt{\left(k_x^2 + k_y^2\right)}$ can be expressed conveniently in terms of the angle of incidence θ_1 as

$$k_{||} = \sqrt{\left(k_x^2 + k_y^2\right)} = k_1 \sin\theta_1 \tag{2.17}$$

which, according to equations 2.16, also allows us to express k_{z1} and k_{z2} in terms of θ_1.

When we apply the boundary conditions (equations 2.12) to the plane incident waves obtained when solving equation 2.11 for each side of the boundary, it follows that the amplitudes of the reflected and transmitted waves can be represented as

$$\begin{aligned} E_{1r}^s &= E_1^s r^s\left(k_x, k_y\right), \quad E_{1r}^p = E_1^p r^p\left(k_x, k_y\right) \\ E_2^s &= E_1^s t^s\left(k_x, k_y\right), \quad E_2^p = E_1^p t^s\left(k_x, k_y\right) \end{aligned} \tag{2.18}$$

where the Fresnel reflection and transmission coefficients are

$$r^s\left(k_x, k_y\right) = \frac{\mu_2 k_{z1} - \mu_1 k_{z2}}{\mu_2 k_{z1} + \mu_1 k_{z2}} \qquad r^p\left(k_x, k_y\right) = \frac{\in_2 k_{z1} - \in_1 k_{z2}}{\in k_{z1} + \in_1 k_{z2}} \tag{2.19}$$

$$t^s\left(k_x, k_y\right) = \frac{2\mu_2 k_{z1}}{\mu_2 k_{z1} + \mu_1 k_{z2}} \qquad t^s\left(k_x, k_y\right) = \frac{2\in_2 k_{z1}}{\mu_2 k_{z1} + \mu_1 k_{z2}} \sqrt{\frac{\in_2 \mu_1}{\in_1 \mu_2}} \tag{2.20}$$

As indicated by the superscripts, these coefficients depend on the polarization of the incident plane wave. The coefficients are functions of k_{z1} and k_{z2}, which can be expressed in terms of k_x , k_y and thus in terms of the angle of incidence θ_1. The sign of the Fresnel coefficients depends on the definition of the electric field vectors shown in Figure 2.6. Then by an analysis of the pointing vector we can find that the reflected and transmitted energy are given by

$$R^{(s,p)} = \left|r^{(s,p)}\right|^2 \tag{2.21}$$

$$T^{(s,p)} = \frac{n_t \cos\theta_t}{n_i \cos\theta_i} \left|t^{(s,p)}\right|^2 \tag{2.22}$$

We can deduce Snell's law of refraction by analyzing the k-vectors continuity in the direction parallel to the boundary. It means

$$k_{||1} = k_{||2} \tag{2.23}$$

Expressed in function of the angle of incidence θ_1 and the angle of transmission θ_t, respectively, we obtain

$$k_1 \sin\theta_1 = k_2 \sin\theta_t \qquad 2.134$$

Where $k_{\mathrm{i}} = 2\pi n_i/\lambda$, with n_i being the i'th medium refractive index and λ the light wavelength. Replacing this on equation 2.20 we obtain Snell's law:

$$n_1 \sin\theta_1 = n_2 \sin\theta_t \qquad 2.145$$

Similarly, when we do the same continuity analysis for the incident and reflected light, where we do not change of medium, we get the reflection expression which says that the reflection angle is equal to the angle of incidence.

$$\theta_1 = \theta_r \qquad 2.156$$

Some information in this section was adapted from Novotny's Book (Ref. 24).

2.3. TOTAL INTERNAL REFLECTION

Total internal reflection is a phenomenon that occurs when the incident medium has a higher refractive index that the transmission medium. As the incident angle increases, the transmitted light bends more and more until it refracts parallel to the surface. The angle of incidence at which this phenomenon takes place is called "critical angle" and if we keep increasing the angle of incidence, there will not be transmitted light.

To calculate the critical angle θ_C we just have to set the transmission angle to 90° in Snell's law. That is:

$$n_1 \sin\theta_C = n_2 \sin 90^\circ \qquad 2.167$$

So the critical angle is

$$\theta_C = \sin^{-1}\frac{n_2}{n_1} \qquad 2.178$$

This phenomenon will occur within the photodetector just if the electros tilt is the adequate.

2.4. REFLECTION IN METALS

The mean characteristic of conducting media is the presence of a number of free electric charges. These charges are electrons in the case of metals, and their motion constitutes a current. The current per unit area results in a conductivity σ different from cero, contrary to the studied media in section 2.2.2. With this consideration, Maxwell's Equations now lead to

$$\frac{\partial^2\vec{E}}{\partial x^2}+\frac{\partial^2\vec{E}}{\partial y^2}+\frac{\partial^2\vec{E}}{\partial z^2}=\mu\epsilon\frac{\partial^2\vec{E}}{\partial t^2}+\mu\sigma\frac{\partial\vec{E}}{\partial t} \quad 2.189$$

which is equation 2.9 in Cartesian coordinates. The last term, is a first-order time derivative, like a damping force in the oscillator model. The time rate-of-change of $\vec{E}$ generates a voltage, currents circulate, and since the material is resistive, light is converted to thermal energy. This expression can be reduced to the non-attenuated wave equation, if the permittivity is reformulated as a complex quantity. This in turn leads to a complex index

$$\tilde{n}=n_R+in_I \quad 2.30$$

where the real and imaginary indices n_R and n_I are both real numbers) into the corresponding solution for a dielectric medium. Alternatively, we can utilize the wave equation and appropriate boundary conditions to yield a specific solution. In either event, it is possible to find a simple sinusoidal plane wave solution applicable within the conductor. Such a wave propagating in the y-direction is ordinarily written as

$$\vec{E}=\overrightarrow{E_0}e^{-\omega n_I y/c}e^{i\omega(t-n_R y/c)} \quad 2.31$$

The expression for reflection over metals is the same than that of dielectrics but considering the imaginary refractive index. The imaginary part represents absorption but also a great enhance in the reflection. That is the reason for metals to reflect light very well and are used ass mirrors.

For our purposes we define Reflection Loss as the non-reflected light by the metal surface due to absorption, this is

$$Reflection\ Loss=1-|r|^2 \quad 2.32$$

In most of the cases a higher imaginary part represents a higher reflection, reducing the reflection losses.

2.5.ANTIREFLECTION LAYERS

The properties of a homogeneous dielectric film situated between two homogeneous media has particular properties of interest in optics, therefore, in this section we are going to study the reflection and transmission coefficients for this system. We assume all the media to be non-magnetic (μ = 1).

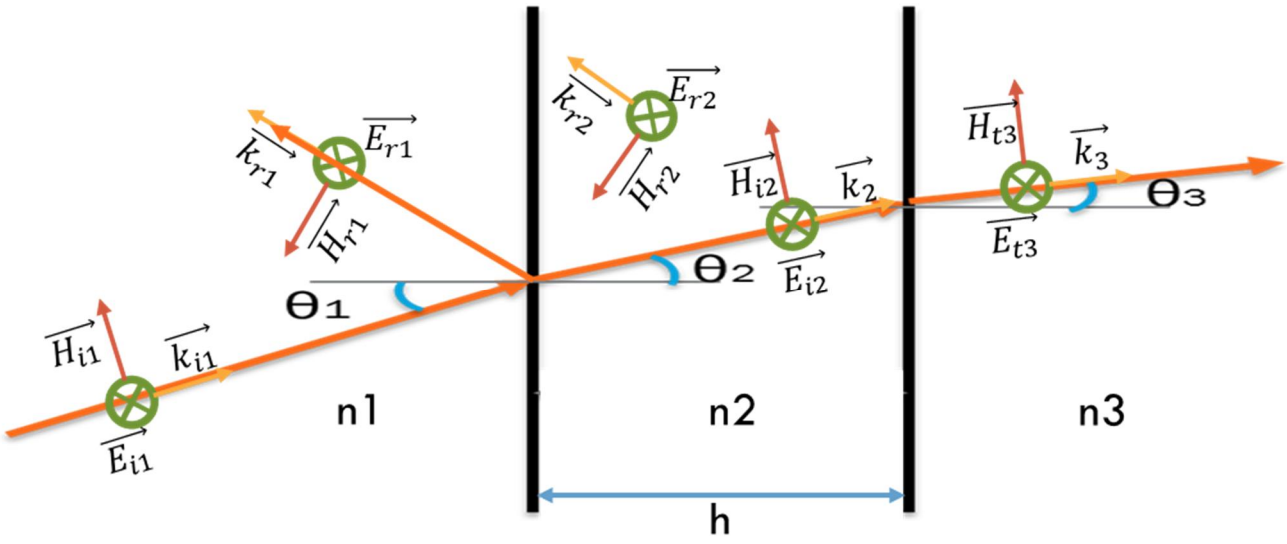

FIGURE 2.7 PROPAGATION OF LIGHT THROUGH A HOMOGENOUS FILM OF AN S-POLARIZED BEAM.

Similarly to the study of the transmission through one single boundary, we can solve analytically Maxwell-s equations for this two-boundary system. As in the one-boundary problem, we can solve it for s-polarized and p-polarized components of the electric field, but here we solve for s-polarized light as shown in Figure 2.7. Subscripts represent the medium where waves are propagating and whether they are incident, reflected or transmitted.

When we apply the boundary conditions for the electric field in the first boundary between n1 and n2, which we name E_I, we get

$$E_I = E_{i1} + E_{r1} = E_{t2} + E'_{r2} \qquad 2.3319$$

Where E'_{r2} represents the wave reflected by the second boundary with a phase shift due to traveling from the second to the first medium. Then when we use Faraday equation (equation 2.3) for a harmonic wave, which means one wavelength and constant amplitude in time, so it takes the form

$$\vec{H} = \sqrt{\frac{\epsilon_0}{\mu_0}} n\vec{k} \times \vec{E} \qquad 2.3420$$

Applying the boundary conditions of the magnetic field to equation 2.34, and expressing the k-vector in terms of the incidence and transmission angles, θ_1 and θ_2 respectively, we get a second equation for the first boundary

$$H_I = \sqrt{\frac{\epsilon_0}{\mu_0}}(E_{i1} - E_{r1}) n_1 \cos\theta_1 = \sqrt{\frac{\epsilon_0}{\mu_0}}(E_{t2} - E_{r2}) n_2 \cos\theta_2 \qquad 2.35$$

Similarly we obtain the following equations for the second boundary, the one between n2 and n3

$$E_{II} = E_{i2} + E_{r2} = E_{t3} \tag{2.36}$$

$$H_{II} = \sqrt{\frac{\epsilon_0}{\mu_0}}(E_{i2} - E_{r2})n_2 \cos\theta_2 = \sqrt{\frac{\epsilon_0}{\mu_0}}(E_{t3})n_3 \cos\theta_3 \tag{2.3721}$$

As we previously mentioned, the electric field suffer a phase shift in the second medium, which is mathematically expressed by an exponential function multiplying the electric field expression. The exponential argument is $k_0 n_2 h \cos\theta_2$, which we will write as $k_0 d$ for simplicity. Adding this phase shift to the fields affected we have

$$\begin{aligned} E_{r2} &= E'_{r2} e^{ik_0 d} \\ E_{i2} &= E_{t2} e^{-ik_0 d} \end{aligned} \tag{2.3822}$$

Substituting these expressions in equations 2.36 and 2.37 we get

$$E_{II} = E_{t2} e^{-ik_0 d} + E'_{r2} e^{ik_0 d} = E_{t3} \tag{2.3923}$$

$$H_{II} = \sqrt{\frac{\epsilon_0}{\mu_0}}\left(E_{t2} e^{-ik_0 d} - E'_{r2} e^{ik_0 d}\right)n_2 \cos\theta_2 = \sqrt{\frac{\epsilon_0}{\mu_0}}(E_{t3})n_3 \cos\theta_3 \tag{2.40}$$

Now, we can see that we have one equality for each of the fields E_I, H_I, E_{II} and H_{II} in terms of E_{t2} and E'_{r2}. For the first boundary it corresponds to the second equality, whereas for the second boundary for the first equality. We can solve for E_{t2} and E'_{r2} the equations system formed by E_{II} and H_{II}, then substitute the results in equations 2.33 and 2.35 obtaining

$$E_I = E_{II} \cos k_0 d + H_{II} \frac{(i \sin k_0 d)}{\sqrt{\frac{\epsilon_0}{\mu_0}} n_2 \cos\theta_2} \tag{2.241}$$

$$H_I = E_{II} \sqrt{\frac{\epsilon_0}{\mu_0}} n_2 \cos\theta_2 \, (i \sin k_0 d) + H_{II} \cos k_0 d \tag{2.425}$$

We then Substitute $\Psi_2 = \sqrt{\frac{\epsilon_0}{\mu_0}} n_2 \cos\theta_2$ and writing equations 2.41 and 2.42 in matrix form

$$\begin{bmatrix} E_I \\ H_I \end{bmatrix} = \begin{bmatrix} \cos k_0 d & i \sin k_0 d/\Psi_2 \\ \Psi_2 i \sin k_0 d & \cos k_0 d \end{bmatrix} \begin{bmatrix} E_{II} \\ H_{II} \end{bmatrix} \tag{2.4326}$$

Now we take the missing equalities of equations 2.33, 2.35, 2.39 and 2.40 and substitute them in equation 2.26 by making the variable changes $\Psi_1 = \sqrt{\frac{\epsilon_0}{\mu_0}} n_1 \cos\theta_1$ and $\Psi_3 = \sqrt{\frac{\epsilon_0}{\mu_0}} n_3 \cos\theta_3$.

$$\begin{bmatrix} E_{i1} + E_{r1} \\ (E_{i1} - E_{r1})\Psi_1 \end{bmatrix} = \begin{bmatrix} \cos k_0 d & i \sin k_0 d/\Psi_2 \\ \Psi_2 i \sin k_0 d & \cos k_0 d \end{bmatrix} \begin{bmatrix} E_{t3} \\ E_{t3}\Psi_3 \end{bmatrix} \tag{2.4427}$$

Expanding the matrix and defining the Fresnel transmission and reflection coefficients as $t^s = {E_{t3}}/{E_{i1}}$ and $r^s = {E_{r1}}/{E_{i1}}$, respectively, we get te following equations system

$$\begin{cases} 1 + r^s = t^s \cos k_0 d + t^s\, i \sin k_0 d\, \Psi_3/\Psi_2 \\ (1 - r^s)\Psi_1 = t^s i \sin k_0 d\, \Psi_2 + t^s \cos k_0 d\, \Psi_3 \end{cases} \quad 2.4528$$

Solving this equations system we get the Fresnel coefficients for a two-boundary system

$$r^s = \frac{\cos k_0 d\, \Psi_1 + i \sin k_0 d\, \Psi_1 \Psi_3/\Psi_2 - i \sin k_0 d\, \Psi_2 - \cos k_0 d\, \Psi_3}{\cos k_0 d\, \Psi_1 + i \sin k_0 d\, \Psi_1 \Psi_3/\Psi_2 + i \sin k_0 d\, \Psi_2 + \cos k_0 d\, \Psi_3} \quad 2.4629$$

$$t^s = \frac{2\Psi_1}{\cos k_0 d\, \Psi_1 + i \sin k_0 d\, \Psi_1 \Psi_3/\Psi_2 + i \sin k_0 d\, \Psi_2 + \cos k_0 d\, \Psi_3} \quad 2.4730$$

A similar process is followed to obtain Fresnel coefficients for p-polarized light. It can be consulted in Born and Wolf's book[25]. And as in the one boundary problem, the reflectance and transmittance are given by.

$$R = |r|^2 \quad 2.4831$$

$$T = \frac{n_1 \cos\theta_1}{n_3 \cos\theta_3} |t|^2 \quad 2.4932$$

For normal incidence all the angles are equal to zero and the reflection coefficient for either s or p polarizations take the form

$$r = \frac{(\mathrm{n}_1 - \mathrm{n}_3)\cos k_0 d + (\mathrm{n}_1 \mathrm{n}_3/\mathrm{n}_2 - \mathrm{n}_2) i \sin k_0 d}{(\mathrm{n}_1 + \mathrm{n}_3)\cos k_0 d + (\mathrm{n}_1 \mathrm{n}_3/\mathrm{n}_2 + \mathrm{n}_2) i \sin k_0 d} \quad 2.5033$$

Multiplying both the numerator and the denominator by n_2 and taking the modulus of r we then have the reflected energy or Reflectance.

$$R = \frac{\mathrm{n}_2^2(\mathrm{n}_1 - \mathrm{n}_3)^2 \cos^2 k_0 d + (\mathrm{n}_1 \mathrm{n}_3 - \mathrm{n}_2^2)^2 \sin^2 k_0 d}{\mathrm{n}_2^2(\mathrm{n}_1 + \mathrm{n}_3)^2 \cos^2 k_0 d + (\mathrm{n}_1 \mathrm{n}_3 + \mathrm{n}_2^2)^2 \sin^2 k_0 d} \quad 2.5134$$

When we make $k_0 d = \pi/2$ to simplify the equation, remembering that $d = n_2 h \cos\theta_2$, it implies that

$$h = \frac{\lambda}{4 n_2} \quad 2.5235$$

And equation 2.32 takes the very simplified form

$$R = \frac{(\mathrm{n}_1 \mathrm{n}_3 - \mathrm{n}_2^2)^2}{(\mathrm{n}_1 \mathrm{n}_3 + \mathrm{n}_2^2)^2} \quad 2.5336$$

[25] M. Born and E. Wolf, Principles of optics: electromagnetic theory of propagation, interference and diffraction of light, Cambridge Univesity Press, 1999.

This becomes zero when

$$n_2 = \sqrt{n_1 n_3} \qquad 2.5437$$

So finally, equations 2.52 and 2.54 are the conditions that a thin film must fulfil to behave as an antireflection layer for normal incidence.

Some information in this section was adapted from reference [25].

CHAPTER 3

3. THE POHOTODETECTOR OPTIMIZATION

In this chapter we are going to analyze part by part the photodetector presented in Figure 1-1. First we are going to select the most convenient metal for the electrodes and then we will continue with study of the Anti-Reflection Layers effects. The whole study is centered in the visible region of the electromagnetic spectrum, which approximately goes from 350 to 800 nanometers of wavelength.

3.1. THE METALLIC ELECTRODES

It is important to choose the most adequate electrodes for the purpose of the new photodetector architecture. We are going to use them not as electrodes only, but as reflectors, so we need them to have a high conductivity and a high reflectance. For that purpose Table 3.1 shows the metals with higher conductivity where we have chosen the higher four to study their optical reflectance.

TABLE 3.1 RESISTIVITY AND CONDUCTIVITY OF HIGHER CONDUCTIVITY METALS. SOURCE: HANDBOOK OF CHEMISTRY AND PHYSICS, 78TH ED[26].

Material	ρ (Ω•m) at 20 °C Resistivity	σ (S/m) at 20 °C Conductivity
Silver	1.59×10^{-8}	6.30×10^{7}
Copper	$1.68\times10^{-}$□	5.96×10□
Gold	$2.44\times10^{-}$□	4.10×10□
Aluminum	$2.82\times10^{-}$□	3.5×10□
Calcium	$3.36\times10^{-}$□	2.98×10□
Tungsten	$5.60\times10^{-}$□	1.79×10□
Zinc	$5.90\times10^{-}$□	1.69×10□
Iron	$1.0\times10^{-}$□	1.00×10□
Platinum	$1.06\times10^{-}$□	9.43×10^{6}
Mercury	$9.8\times10^{-}$□	1.02×10^{6}

Following the parameters of the photodetector proposed by Pieter G. Kik in [10], the electrodes cover material has a refractive index of $n_{CV} = 2$, so using this along with the metals

[26] W. M. Haynes, Handbook of Chemistry and Physics, CRC, 2014-2015.

refractive indexes for a wavelength $\lambda = 563.6$nm (Palik's Data[27]), which corresponds to the central wavelength of the visible spectrum, we plotted the reflection Loss (equation 2.32) of each metal varying the angle of incidence in Figure 3.1. When comparing these plots, it is evident that Silver is the best reflector at any incidence angle for 563.6nm light. It is important to notice that a higher conductivity does not means a higher reflectance, for example copper has a higher conductivity than Aluminum and Gold, but has a poor reflection. Also we can see that TM polarized light is always more absorbed than TE polarized in angles different from 0° and 90° degrees, and it reaches a maximum at what is now called "principal angle of incidence". The behavior of unpolarized light remains almost constant over the first degrees, for example in Silver there is not a big difference of unpolarized light from 0° to 50° of incidence.

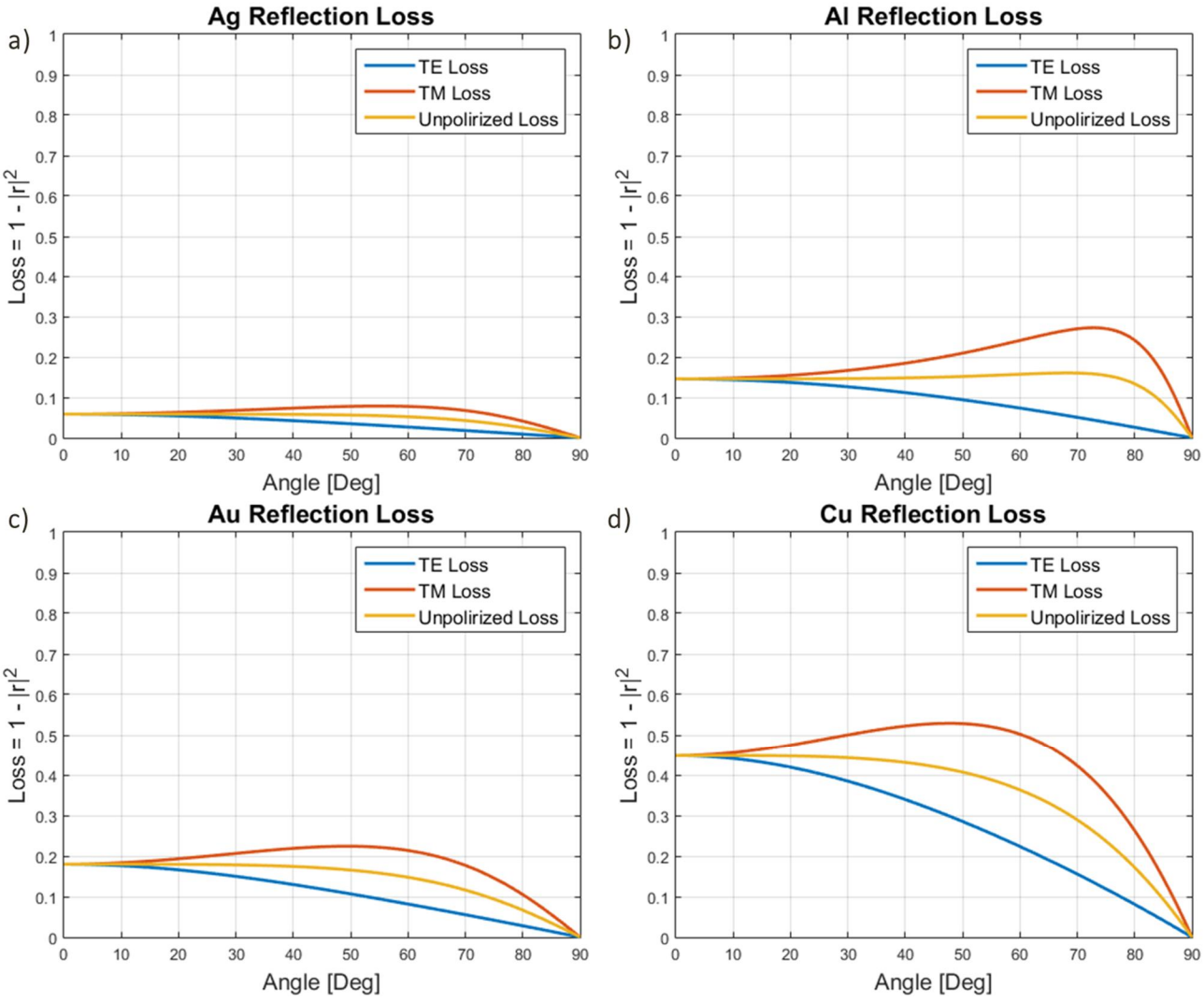

FIGURE 3.1 REFLECTION LOSS AT 563.6 NM OF WAVELENGTH FOR A) SILVER, B) ALUMINUM, C) GOLD AND D) COPPER.

[27][Online].Available:https://code.google.com/p/lampsolar/source/browse/trunk/data/optical_constants/?r=915#optical_constants. [Accessed 06 May 2015].

So Silver is our favorite metal for 550nm, but we can also compare these metals behavior for a wide range of wavelengths, in other words, to compare their loss spectrum. We can see in Figure 3.2 that although Aluminum is a better reflector for the UV region compared to the other three metals, Silver has a fast drop and becomes better than Aluminum around 425nm. This plot is clearly visible in daily life, aluminum is widely used for mirrors fabrication and so is Silver, in these two metals we can see our clear reflection and their color is actually silver, while Gold looks yellow and Copper reddish, corresponding to the wavelengths they reflect.

We can conclude here that Aluminum is the best option for wide spectrum detection, whereas Silver is convenient for wavelengths over 400nm. In this work we have chosen silver because in most of the visible region is quite better than Aluminum.

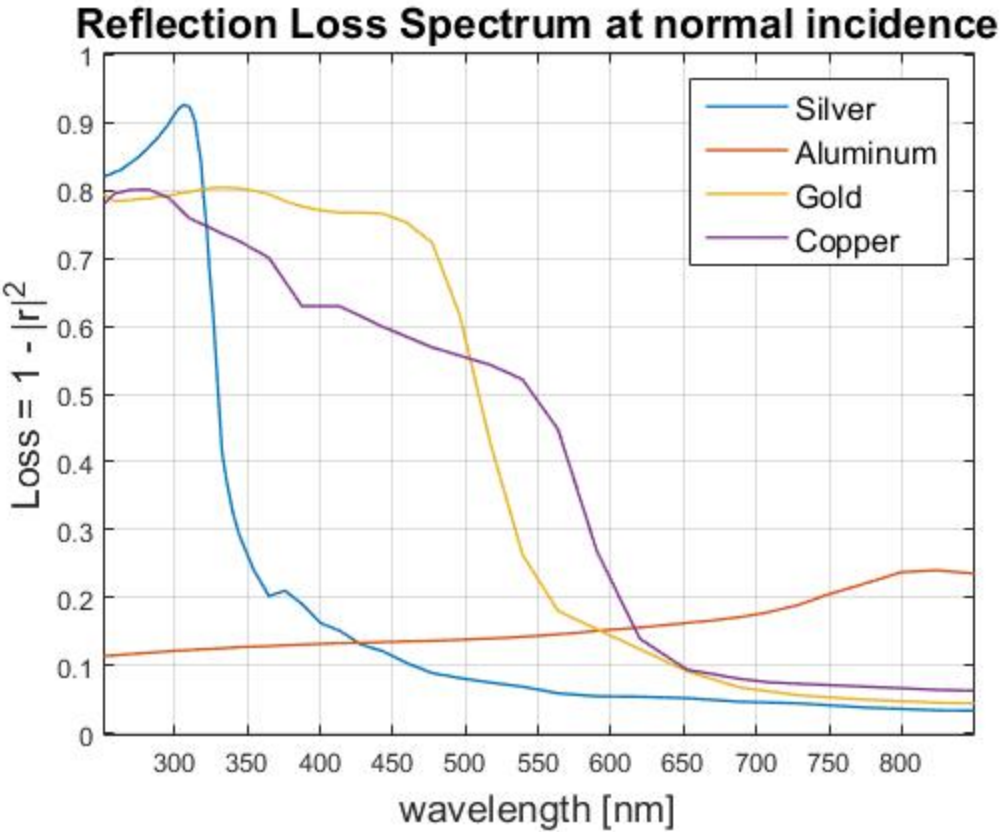

FIGURE 3.2 REFLECTION LOSS AT DIFFERENT WAVELENGTHS FOR SILVER(BLUE LINE), ALUMINUM (RED LINE), GOLD (YELLOW LINE) AND COPPER(PURPLE LINE).

Now that we have chosen the electrodes material, we proceed to make a geometrical analysis of light path when it travels through the embedded electrodes photodetector.

3.2. GEOMETRICAL ANALYSIS

Before a physical study of the interaction of light with the photodetector, we will see in this section the path that straight light rays would follow into the photodetector when they fall normally upon the photodetector's surface.

Initially we consider the embedded photodetector without any Anti-Reflection Layer (ARL) in Figure 3.3, where brown lines help us to see the angles correspondence. The tilt of the electrodes is represented by the Greek letter theta (θ). We can see that there is a brown cross made by the normal incident light and the horizon. If we rotate this cross in θ degrees, the electrode's surface tilt, we arrive to the green cross made by the electrode's surface and the normal to this surface. Here we can see that the angle of incidence of light over electrode's surface is equal to that of the electrode's surface tilt and according to the reflection law (equation 2.26) the angle of incidence is equal to the angle of reflection. So light is deviated in 2θ degrees after reflection and we have that this deviation angle is alternate interior angle with the second incidence angle so they are equal. This second incidence angle is important because it has to be bigger than the critical angle in order that we have TIR. Mathematically the minimum tilt angle required for TIR is

$$\theta_{min} = \theta_c/2 \qquad 3.1$$

Where θ_c is the critical angle.

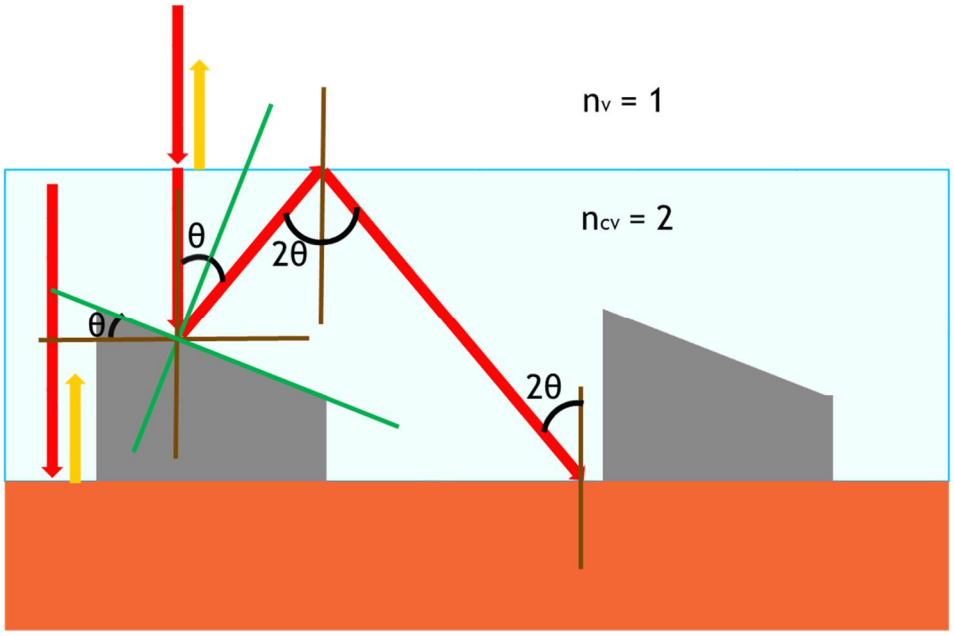

FIGURE 3.3 GEOMETRICAL ANALYSIS OF NORMAL INCIDENT LIGHT IN THE EMBEDDED PHOTODETECTOR.

So using equation 2.28 we easily calculate the critical angle having transmission an incidence refractive indexes of $n_v = 1$ and $n_{cv} = 2$ respectively.

$$\theta_c = \sin^{-1}\frac{1}{2} = 30° \tag{3.2}$$

Now from equation 3.1 it is easy to see that the minimum tilt angle is

$$\theta_{min} = 15° \tag{3.3}$$

But for a better TIR, we have chosen a ***tilt of 20°***.

Now that the tilt has been chosen, we may notice that if the cover height surpass the electrodes surface in a large distance, the Total Internal Reflected Light (TIRL) may be directed to another electrode surface and keep bouncing indefinitely between the cover and the electrodes. If the cover surface is very close to the electrodes, then some TIRL will bounce back to the electrode surface and won't reach the semiconductor. So there is an ideal cover height where incoming light reflected by the left side of the electrode bounces to its right side and the incoming light reflected by the electrode's right side bounces to the next electrode's left side as it is shown if Figure 3.4.

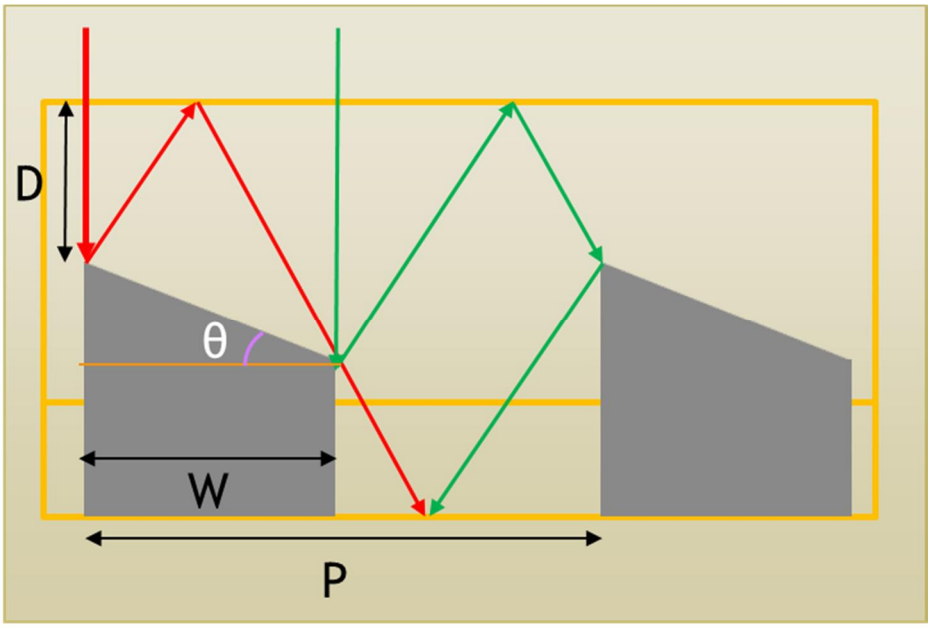

FIGURE 3.4 IDEAL COVER THICKNESS DIAGRAM FOR AN EMBEDDED ELECTRODES PHOTODETECTOR.

At 50% metal coverage (W = P/2), the ideal cover height "D" is related to the electrodes period "P" by[18]

$$D = \frac{1}{4}(\cot 2\theta - \tan\theta)P \tag{3.4}$$

where θ is the electrodes tilt.

The previous analysis works perfectly when we do not have the top ARL, but once we put the ARL we may wonder if the critical angle whether stills the same or not. It can be easily answered by using Snell's law (equation 2.25). We have that Snell's law is fulfilled for each boundary as it is shown in Figure 3.5, where "$n_1 \sin\theta_1 = n_2 \sin\theta_2$" and "$n_2 \sin\theta_2 = n_3 \sin\theta_3$" for the bottom and

the top boundaries respectively. Thus we get by transitivity that "$n_1 \sin\theta_1 = n_3 \sin\theta_3$", which means that we can ignore the inner medium and the critical angle remains equal. It happens when the refractive indexes fulfill $n_1 > n_2 > n_3$.

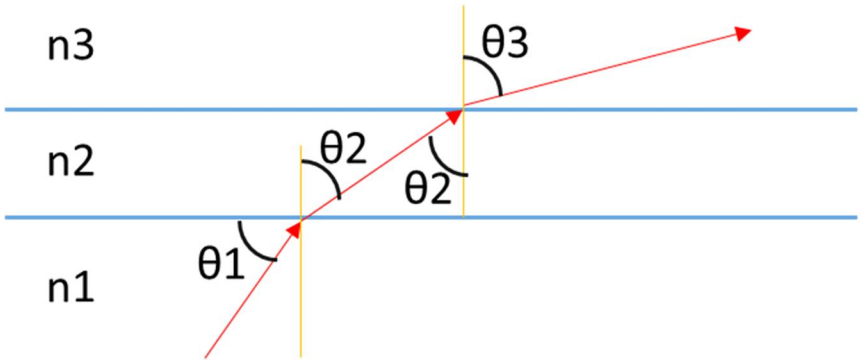

FIGURE 3.5 LIGHT TRAVELING THROUGH A TIN FILM, NOTICE IN THE SECOND MEDIUM THAT TRANSMISSION ANGLE AND INCIDENT ANGLE ARE EQUAL.

The ARL also induce light to suffer a small shift caused by refraction and thus the height is not the optimum anymore (Figure 3.6 (a)). To recover the condition of total transmission it is necessary to adjust the cover height as shown in Figure 3.6 (b) and we can calculate this adjust "d" trigonometrically.

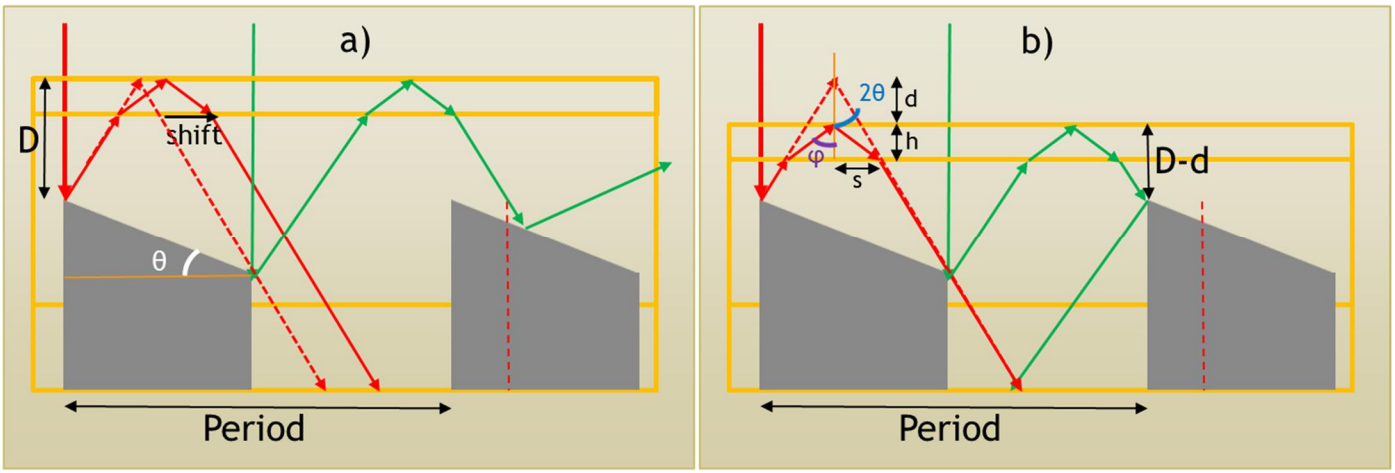

FIGURE 3.6 A) THE EMBEDDED ELECTRODE SHIFT EFFECT CAUSED BY THE TOP ARL AND B) THE HEIGHT ADJUSTMENT TO KEEP THE TOTAL TRANSMISSION CONDITION.

Taking advantage of the right triangle in Figure 3.6 (b), it is easy to establish a relation between the adjust "d" with the ARL thickness "h", the triangle base or shift "s" and the tilt "θ" in the form:

$$\tan 2\theta = \frac{s}{d+h} \qquad 3.5$$

where

$$d = \frac{s}{\tan 2\theta} - h \tag{3.6}$$

Now “s” can be calculated using the right triangle of height “h”, where the upper angle “φ” can be calculated by Snell’s law. We know that the incident angle to the ARL is equal to twice de tilt so we have

$$n_{CV} \sin 2\theta = n_{ARL} \sin \varphi \tag{3.7}$$

$$\varphi = \sin^{-1}\left(\frac{n_{CV}}{n_{ARL}} \sin 2\theta\right) \tag{3.8}$$

and for “s” we have

$$\tan \varphi = \frac{s}{h} \tag{3.9}$$

replacing φ we get

$$s = h \tan\left[\sin^{-1}\left(\frac{n_{CV}}{n_{ARL}} \sin 2\theta\right)\right] \tag{3.10}$$

using trigonometrical identities we can write every trigonometric function in terms of sine

$$s = h \frac{\sin\left[\sin^{-1}\left(\frac{n_{CV}}{n_{ARL}} \sin 2\theta\right)\right]}{\sqrt{1 - \sin^2\left[\sin^{-1}\left(\frac{n_{CV}}{n_{ARL}} \sin 2\theta\right)\right]}} \tag{3.11}$$

$$s = h \frac{\frac{n_{CV}}{n_{ARL}} \sin 2\theta}{\sqrt{1 - \left(\frac{n_{CV}}{n_{ARL}} \sin 2\theta\right)^2}} \tag{3.12}$$

simplifying

$$s = \frac{h n_{CV} \sin 2\theta}{\sqrt{n_{ARL}^2 - n_{CV}^2 \sin^2 2\theta}} \tag{3.13}$$

Now we can replace the result of equation 3.13 in equation 3.6 to obtain

$$d = \frac{\frac{h n_{CV} \sin 2\theta}{\sqrt{n_{ARL}^2 - n_{CV}^2 \sin^2 2\theta}}}{\tan 2\theta} - h \tag{3.14}$$

and replacing the tangent with sine over cosine we finally get

$$d = \frac{h n_{CV} \cos 2\theta}{\sqrt{n_{ARL}^2 - n_{CV}^2 \sin^2 2\theta}} - h \qquad 3.15$$

So the ideal cover thickness, including the top ARL, for a 50% metal coverage photodetector has to be diminished a distance "d", thus

$$D = \frac{1}{4}(\cot 2\theta - \tan\theta)P - h\left(\frac{n_{CV} \cos 2\theta}{\sqrt{n_{ARL}^2 - n_{CV}^2 \sin^2 2\theta}} - 1\right) \qquad 3.16$$

So we can see that if the ARL thickness is zero, we recover the original cover height. If we consider our photodetector with a top ARL refractive index $n_{ARL} = \sqrt{n_{CV} n_V}$, with $n_V = 1$ (vacuum refractive index), $n_{CV} = 2$, $\theta = 20°$, and thickness $h = 550nm/4n_{ARL} = 97.227nm$ the distance adjustment is

$$d = h\left(\frac{n_{CV} \cos 2\theta}{\sqrt{n_{ARL}^2 - n_{CV}^2 \sin^2 2\theta}} - 1\right) = 97.227nm\left(\frac{2\cos 40°}{\sqrt{2 - 2^2 \sin^2 40°}} - 1\right) \qquad 3.17$$

$$\boldsymbol{d = 155.5632nm} \qquad 3.18$$

Which can be negligible for large photodetectors, but if the period is of two microns for example, then it becomes indispensable to take the shift into account.

3.3. THE TOP ANTI-REFLECTION LAYER (TARL)

The TARL is the front external cover of the photodetector and is used to eliminate the light reflected by the surface. We can easily select an ARL for a single wavelength at a single angle of incidence using equations 2.52 and 2.54, but here we are going to choose the most convenient ARL for wide angle and spectrum detection.

550 nm is the central wavelength of our detection spectrum, so for normal incidence the ideal TARL refractive index is $n_{ARL} = \sqrt{2}$, which implies an ideal thickness of $h = 97.227nm$. With this parameters we proceed to analyze the transmission at different angles of incidence.

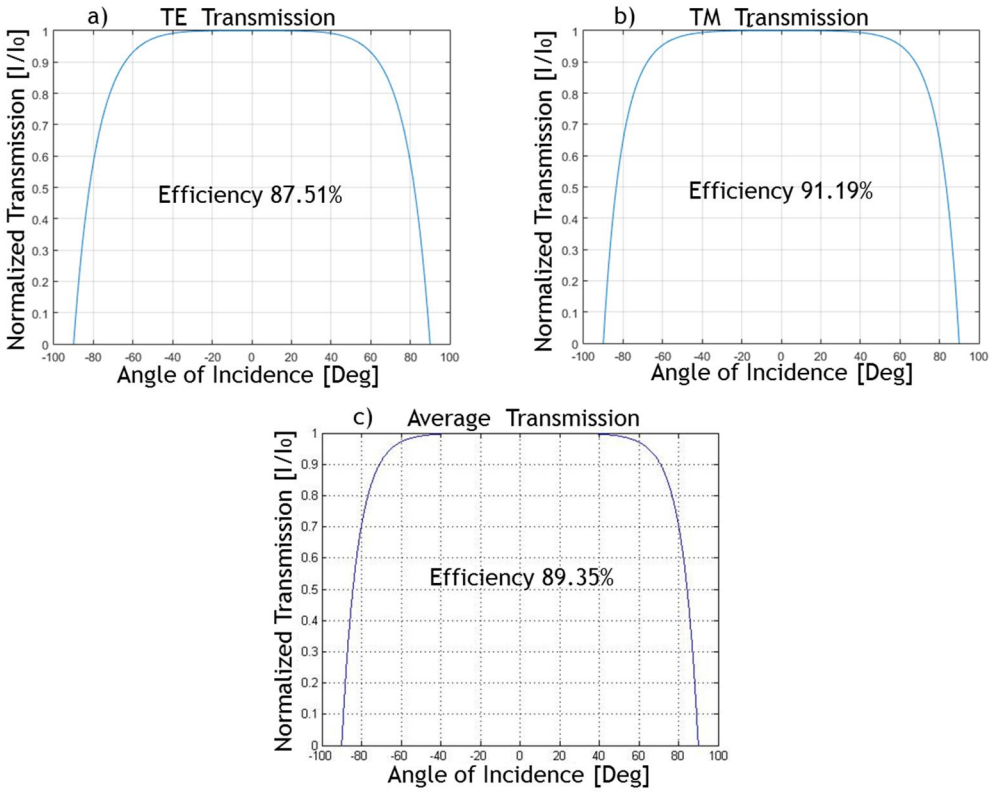

FIGURE 3.7 WIDE ANGLE TRANSMISSION FOR A) TE, B)TM POLARIZATIONS AND C) UNPOLARIZED LIGHT THROUGH A THIN FILM.

Using equation 2.49 we obtained the plots shown in Figure 3.7, where we see that for both polarizations the transmission is almost 100% near to the normal incidence and it has a fast decay at ±60° for TM polarization (Figure 3.7 (a)) and at around ±45° for TE (Figure 3.7 (b)), the average transmission is the sum of both polarizations transmissions divided by two (Figure 3.7 (c)). I proposed the efficiency as a figure of merit to compare the wide angle transmissions, which is defined as the proportional area under the transmission curve. This efficiency is specified in each plot and the TM polarization presents a better transmission than the TE.

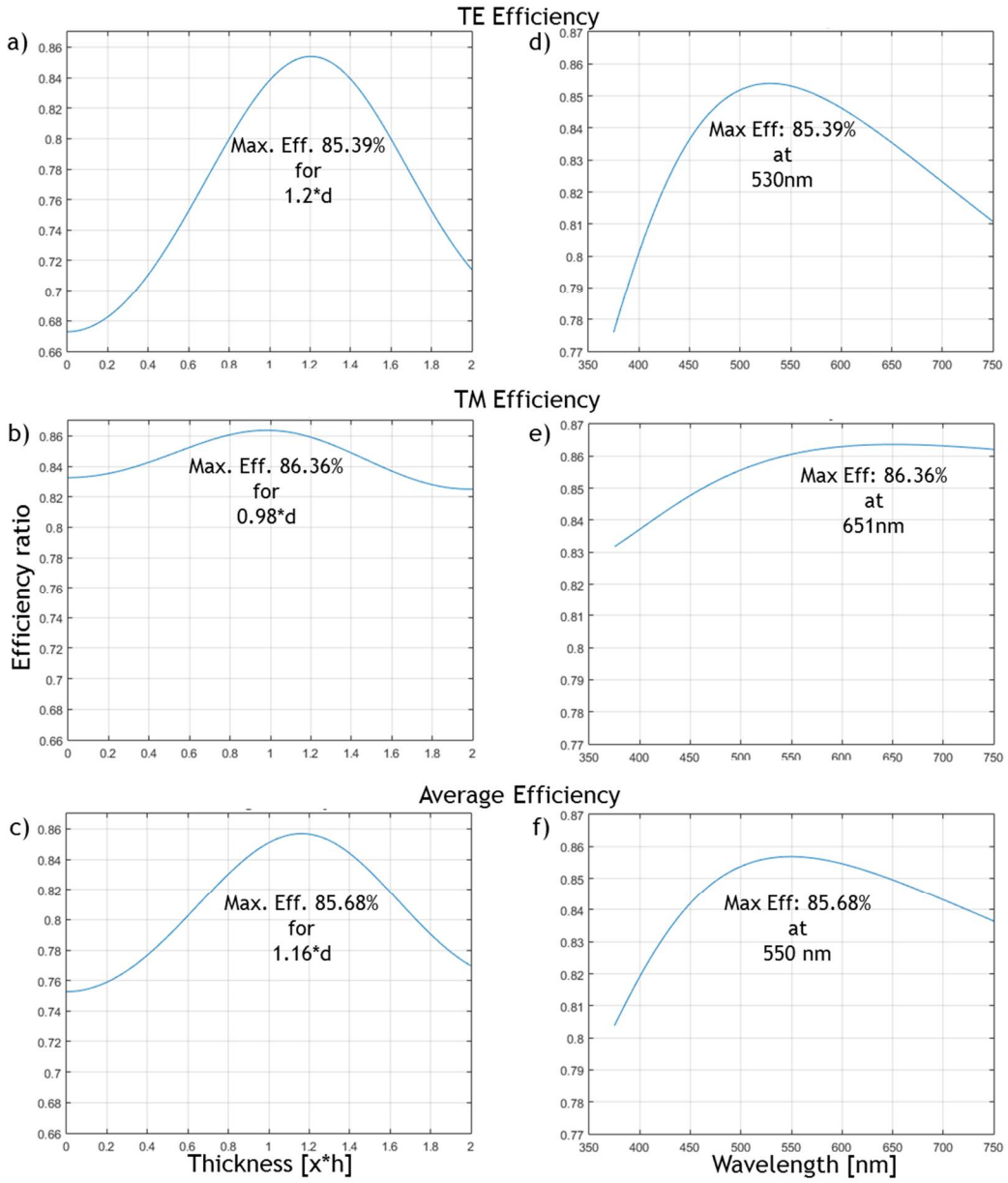

FIGURE 3.8 STUDY OF THE TRANSMISSION EFFICIENCY FOR DIFFERENT ARL THICKNESES IN A)TE, B)TM AND C)UNPOLARIZED LIGHT. AND EFFICIENCY FOR DIFFERENT WAVELETHS WITH AN ARL THICKNESS OF 1.13 TIMES THE IDEAL FOR 550 NM.

Even when the transmission is quite good using the ideal thickness for normal incidence, it is not the best option for wide angle detection. To calculate the best TARL thickness we plotted the efficiency for different thicknesses and the results are presented in Figure 3.8 (a), (b) and (c). The thickness in 'x' axis is a factor of the normal ideal thickness, so $x = 1$ represents the ideal thickness $h_{TARL} = 97.227nm$. For TE polarization the maximum efficiency reached is 85.39% and lies in $x = 1.2 \times h_{TARL}$, whereas TM maximum efficiency is 86.36% at $x = 0.98 \times h_{TARL}$. It is a very different maximum efficiency thickness for each polarization, so we can design ARLs that preferably works for one polarization. Always TM reaches a higher transmission than TE, but we will consider

unpolarized light, so we take the average transmission efficiency plotted in Figure 3.8 (c), where the maximum efficiency is **85.68%** at thickness $\boldsymbol{x = 1.16 \times h_{TARL}}$.

Once we choose the best TARL thickness for 550nm, we can proceed to study the efficiency of this layer for other wavelengths. The efficiency in function of the wavelength is plotted in Figure 3.8 (d),(e) and (f) for different polarizations. We have a transmission efficiency between 80% and 86% for unpolarized light with a maximum at 550 nm. Again we can see that TM polarization curve presents the best behavior along the visible spectrum, so here we can learn that for wide angle and wide spectrum ARLs it is always more convenient to use TM polarized light for a better transmission.

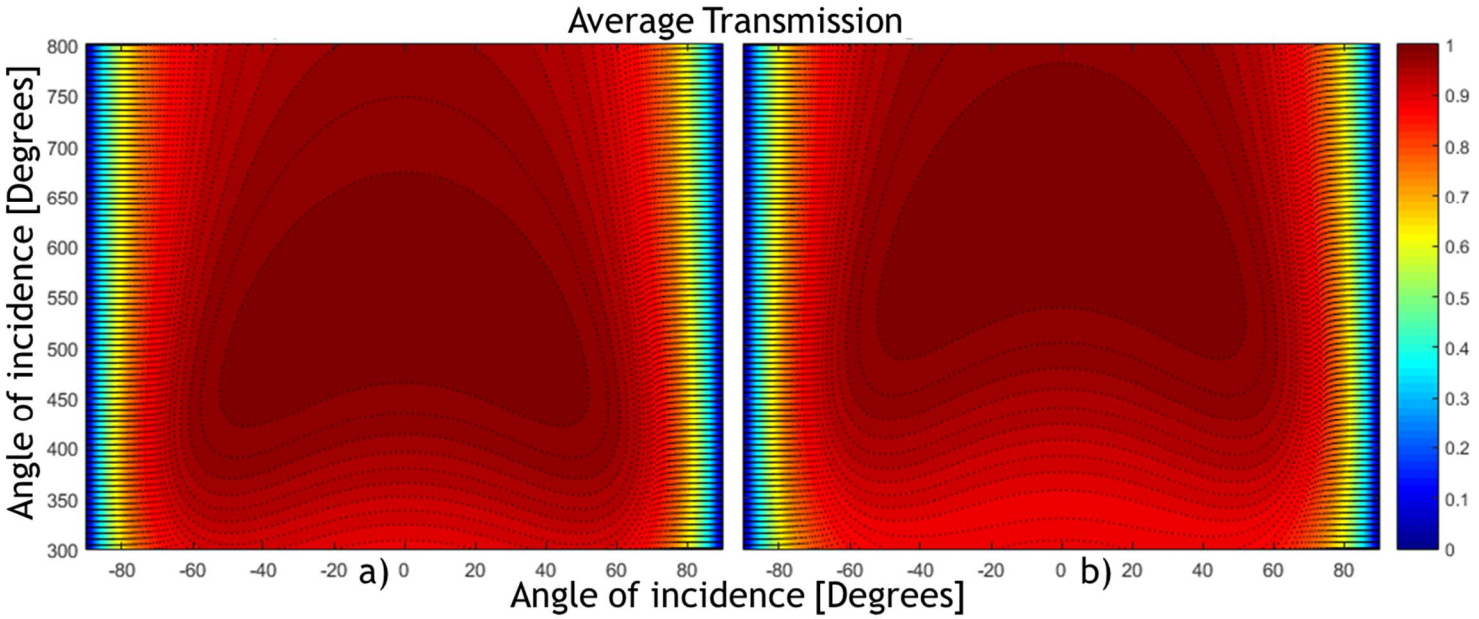

FIGURE 3.9 CONTOUR PLOT OF THE TRANSMISSION IN FUNCTION OF THE WAVELENGTH AND THE ANGLE OF INCIDENCE FOR THROUGH AN ARL OF THICKNESS A) H=97.227NM AND B) H=112.783NM.

Figure 3.9 give us a better visualization of the transmission through the TARL in two cases, (a) when the TARL thickness is the ideal for normal incidence of 550 nm light ($h_{TARL} = 97.227nm$), and (b) when the thickness is 1.16 times h_{TARL}, which corresponds to the thickness that gave us more efficiency. Here we can notice that that higher transmission region (in red) shifts up as we increase the thickness and shifts down when we decrease it. By selecting the more efficient ARL thickness we can see that the higher transmission region also grows a little in size, so we have a better transmission for more wavelengths and more angles.

Here we conclude with the selection of the best TARL for wide angle detection and we will continue with the study of the ARL over a lossy medium.

3.4. THE BOTTOM ANTI-REFLECTION LAYER (BARL)

Thin layers can also be used to increase or decrease the reflection over lossy medium. We call BARL to the antireflection layer which lies upon the semiconductor. Unlike non lossy media antireflection layers, there is not a popular general rule to select an ideal refractive index for lossy media ARL, so in this section we studied numerically several refractive index values for a constant BARL height over silicon, which is a lossy material of index $n_S = 4.07926 + i0.0370459$ for light of 550 nm.

In principle, we know that the polarization of incident light changes after being reflected by metals and the interference is not equal to that of non lossy media, then we can try to find the varying the ARL height or its refractive index. We decided to fix the thickness and vary the refractive index real and imaginary part with the purpose of learn if the ARL for lossy media should be also lossy or not.

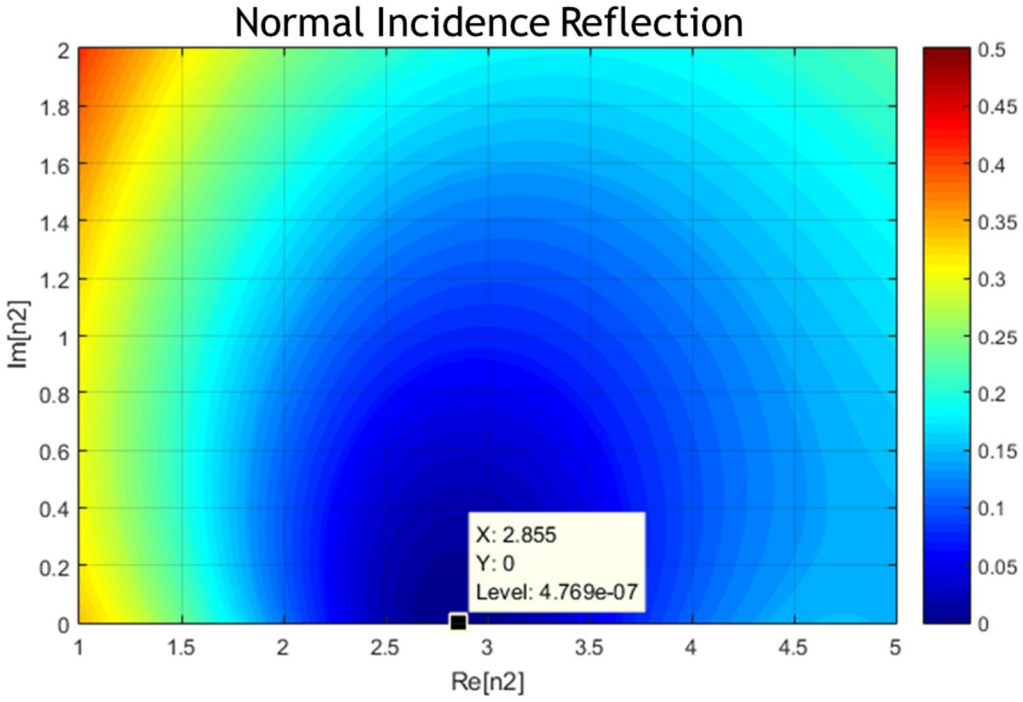

FIGURE 3.10 REFLECTION OVER THE BARL FOR 550 NM VARYIN THE BARL REFRCTIVE INDEX IMAGINARY AN REAL PARTS. THERE IS A DATATIP MARKING THE LOWER REFLECTION.

Using the trial and error method we studied the refraction index for many BARL heights, and we found that the reflection becomes closer to zero for the thickness is $h_{BARL} = \frac{5\ 5 0 m}{4 \times 2.88} = 47.74nm$. Figure 3.10 shows the contour plot obtained for the transmission using the mentioned thickness and at normal incidence, 'y' axis is the imaginary part of the BARL refractive index ant 'x' axis the real part. We can notice that the higher reflection occurs when $n_{BARL} = 2.855$, a real value which means that the BARL should be non lossy so we can reduce the reflections to zero, because if we increase the imaginary part then the reflection grows.

We may remember that the light reflected by the electrodes fall upon the semiconductor at twice the tilt angle, thus we study in Figure 3.11 the reflection of the BARL at different angles and wide spectrum taking the aluminum data from Palik's[26]. The darker blue region represents a reflection lower than 2.0%, so we notice a very nice low reflection for a wide angle and many wavelengths, specifically in an incidence of 40 degree the BALR keeps a wide spectrum good behavior.

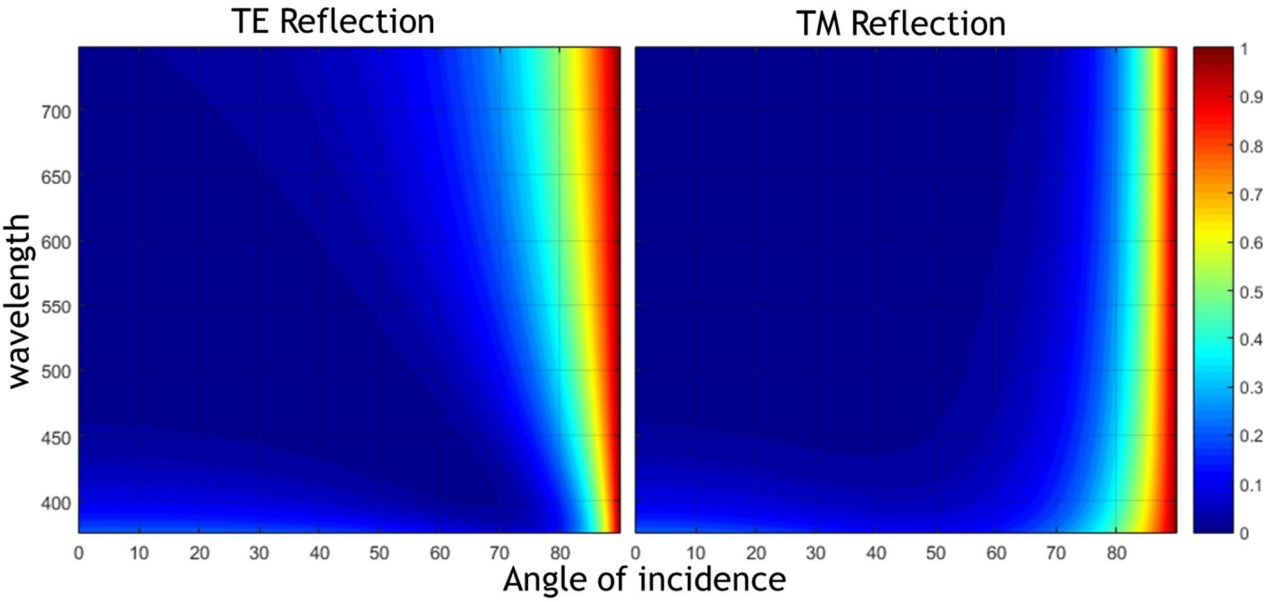

FIGURE 3.11 REFLECTION OF THE BARL AT DIFFERENT ANGLES OF INCIDENCE AND WIDE SPECTRUM FOR TE AND TM POLARIZATIONS.

This low reflection assure us that most of the light is breaking through the photodetector structure to reach the semiconductor that in this case is silicon.

CHAPTER 4

4. SIMULATION RESULTS

CST STUDIO SUITE® (CST) is a software that offers accurate, efficient computational solutions for electromagnetic design and analysis. Its 3D electromagnetic simulation software enables you to choose the most appropriate method for the design and optimization of devices operating in a wide range of frequencies. We used the tetrahedral mesh feature which uses the finite differentials method.

Before starting the simulations I did some trials to compare the results launched by CST with my own MATLAB code. First for an ARL between non lossy media with refractive indexes $n_V = 1.0$, $n_{ARL} = \sqrt{1.5}$ and $n_{GLASS} = 1.5$ in that order, with an ARL height of $h_{ARL} = 550nm/(4 \times n_{ARL})$. We plotted reflection vs wavelength for angles of incidence of 0°, 30° and 60°. The results are shown in Figure 4.1, where the dash lines are the CST results and the solid line are MATLAB results. The lines are equal and thus we proved the validity of both methods for non lossy media.

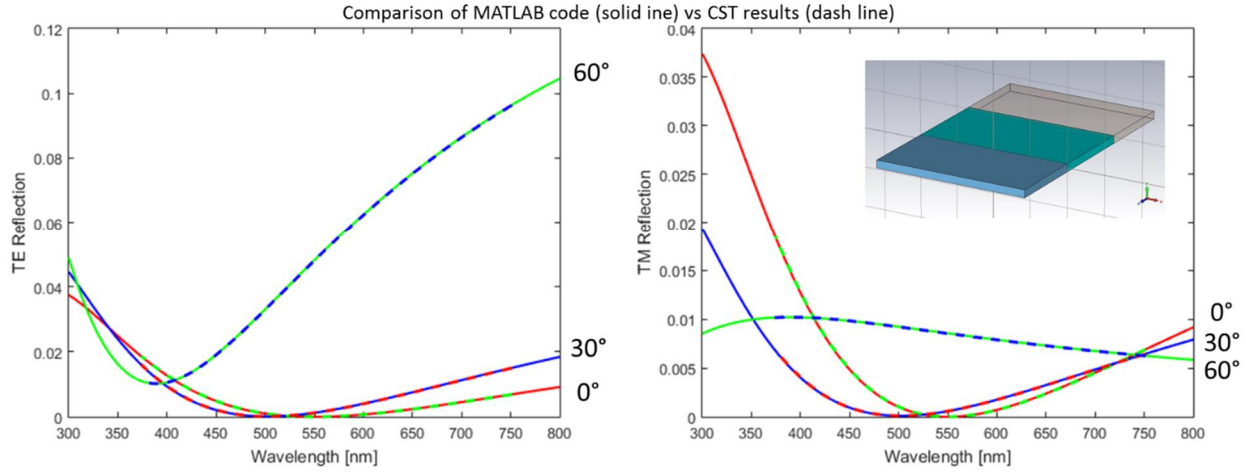

FIGURE 4.1 REFLECTION FROM AN ARL FOR INCIDENCE ANGLES OF 0, 30 AND 60 DEGREES. RESULTS FROM CST STUDIO SUITE (DASH LINE) AND MATLAB (SOLID LINE) ARE SHOWN TO COMPARE. THE ARL SCHEME IS IN THE TOP-RIGHT CORNER.

CST software works through ports, one is the entrance and the other is the exit, and it doesn't work when any of the ports is a lossy medium, thus we had to simulate a photodetector where everything is non lossy but the electrodes. The proposed device consists in a stack of refractive indexes of **1.0 - 1.414 - 2 - 2.828 – 4** in that order, which almost corresponds **to Air-Silicon Dioxide (SiO_2)-Silicon Nitride (Si_3N_4)-Silicon Carbide (SiC)- Silicon (Si)** for the visible spectrum respectively. Silver tilted electrodes are covering 50% of the Silicon with a period $P = 2000nm$ (Figure 4.2).

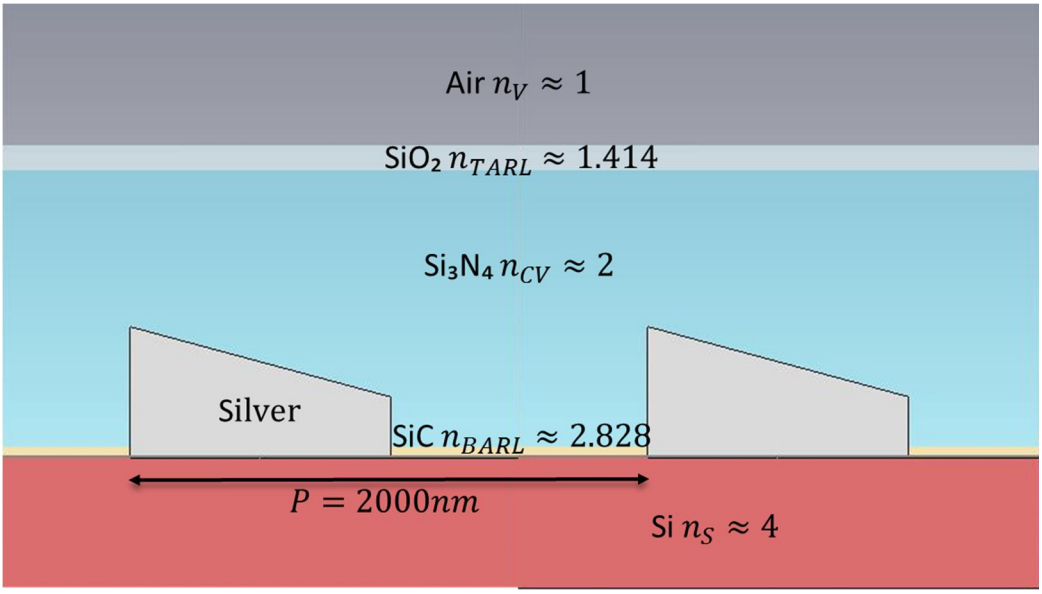

FIGURE 4.2 EMBEDDED ELECTRODES PHOTODETECTOR DESIGN FOR SIMULATIONS. THE ELECTRODES TILT IS OF 20°.

Simulations were done for many photodetector configurations in order to compare their behavior and using one period of the configuration as a unit cell. Coming up next are the unit cell images and its simulation results followed by their interpretation.

4.1. BASIC EMBEDDED ELECTRODE

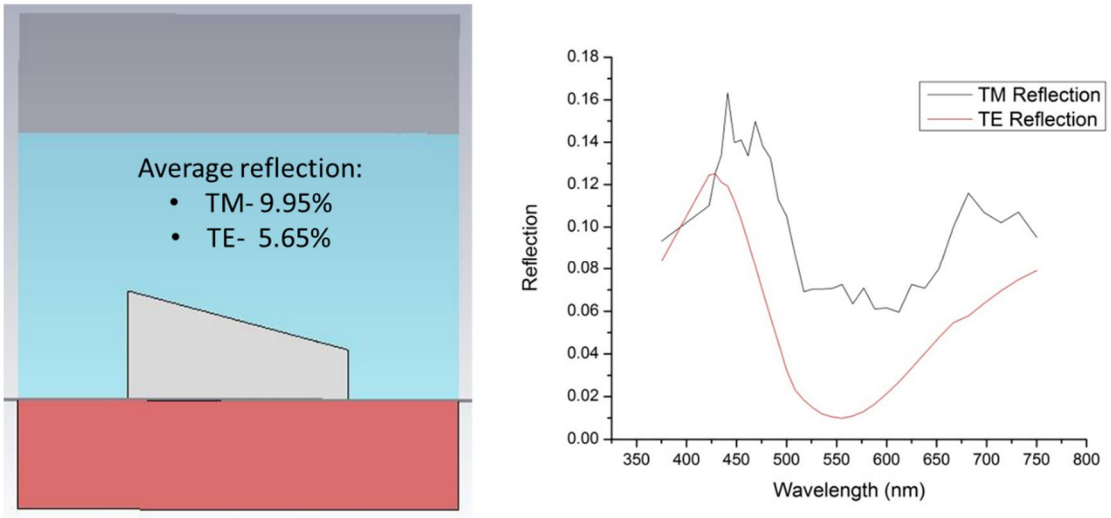

FIGURE 4.3 SIMULATION RESULTS FOR THE BASIC EMBEDDED PHOTODETECTOR.

This is the simplest embedded electrode configuration and its cover height is calculated with Equation 3.4. We can notice that the reflection is quite low for both polarizations, especially for TE. Therefore it confirms the effectiveness of the embedded photodetector design. Next we will see what happen after the implementation of the TARL.

4.2. EMBEDDED ELECTRODE WITH TARL

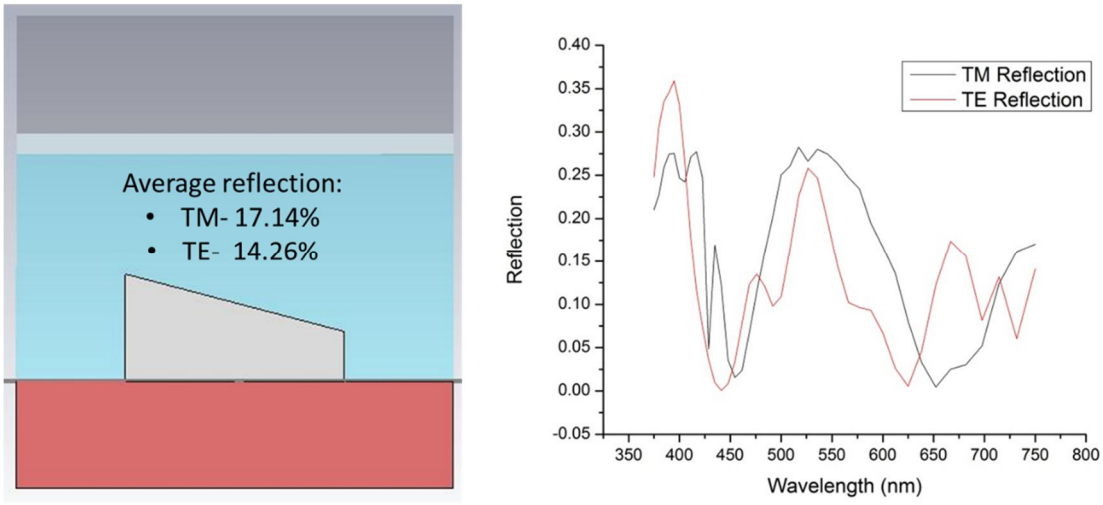

FIGURE 4.4 SIMULATION RESULTS FOR THE EMBEDDED PHOTODETECTOR AFTER THE IMPLEMENTATION OF THE TARL.

Even with the implementation of the TARL, we see in Figure 4.4 that the reflection increases contrary to the desired result. The reason for this undesired behavior is that the cover height was not adjusted, therefore a fraction of light just keep bouncing from electrode to electrode until it is completely absorbed. In addition there is a big difference between cover and semiconductor refractive indexes, which results in a high reflection in that boundary.

4.3. EMBEDDED ELECTRODE WITH BARL

There is a lot of weird oscillations especially for TM polarizations, but it is due to the short scale presented in the Figure 4.5 for the reflection. If we increase the scale it looks like a straight line. In this case the BARL and the cover are ideal and the low amount of reflected light is principally due to the boundary between air and the cover medium.

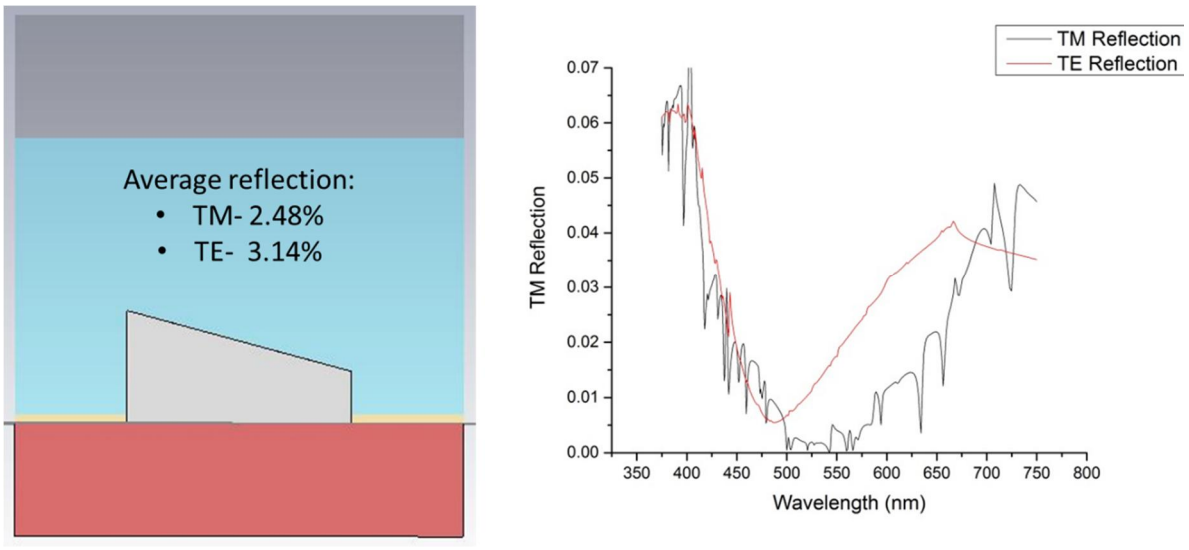

FIGURE 4.5 SIMULATION RESULTS FOR THE EMBEDDED PHOTODETECTOR AFTER THE IMPLEMENTATION OF THE BARL.

4.4. EMBEDDED ELECTRODE WITH TARL AND BARLS

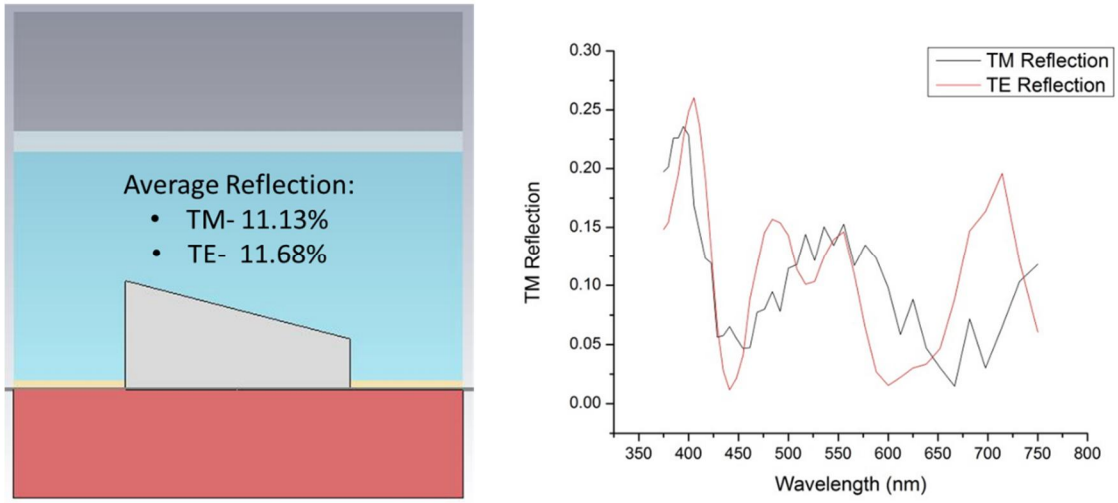

FIGURE 4.6 SIMULATION RESULTS FOR THE EMBEDDED PHOTODETECTOR AFTER THE IMPLEMENTATION BOTH TARL AND BARL.

In Figure 4.6 we can see again that the implantation of the TARL increases the reflection instead of damp it. The reason is the same that in Figure 4.4, and it is because there was not considered the cover height adjustment. These two figures confirm our results from the

CHAPTER 5

5. CONCLUSIONS

We have demonstrated that the implementation of a TARL to the embedded photodetector introduced by Dr. Pieter G. Kik can behave against or in favor of the photodetector performance. Whereas the implementation of a BARL is always very helpful because it does not cause any deviation of light that could break with the ideal transmission condition.

To use the TARL in favor of the photodetector transmission, the cover height has to be adjusted according to equation 3.16, which is maybe the most important result of this thesis.

Through the implementation of this kind of photodetectors, light would not be wasted by reflection on top electrodes and this would become very useful in applications where light is very limited, like communications and more generally in Very Large Scale Integration circuits (VLSI).

Usually the electrodes coverage is of 33.33% over the semiconductor as in the patent of Ref. [1]. It was for increasing the depletion region and improve the carriers creation quantum efficiency, but the farther the electrodes, the weaker the weaker the voltage and thus, the lower response speed. With the embedded photodetector, electrodes can be closer intensifying the voltage between them and keep taking advantage of almost the whole incident light, leading to an optimum response speed and a high improvement of the quantum efficiency.

REFERENCES

[1] H. C. Lee and B. Van Zeghbroeck, "A novel high-speed silicon MSM photodetector operating at 830 nm wavelength," *Electron Device Letters, IEEE,* vol. 16, no. 5, pp. 175-177, 1995.

[2] J. B. Soole and H. Schumacher, "InGaAs metal-semiconductor-metal photodetectors for long wavelength optical communications," *IEEE Journal of Quantum Electronics,* vol. 27, no. 3, pp. 737-752, 1991.

[3] J. H. Kim, H. T. Griem, R. A. Friedman, E. Y. Chan and S. Ray, "High-performance back-illuminated InGaAs/InAlAs MSM photodetector with a record responsivity of 0.96 A/W," *IEEE Photonics Technology Letters,* vol. 4, no. 11, pp. 1241-1244, 1992.

[4] F. Omnès, E. Monroy, E. Muñoz and J.-L. Reverchon, "Wide bandgap UV photodetectors : A short review of devices and applications," *In Integrated Optoelectronic Devices 2007. International Society for Optics and Photonics,* vol. 6473, p. 6473E, 2007.

[5] A. Müller, G. Konstantinidis, M. Dragoman, D. Neculoiu, A. Dinescu, M. Androulidaki, M. Kayambaki, A. Stavrinidis, D. Vasilache, C. Buiculescu, I. Petrini, C. Anton, D. Dascalu and A. Kostopoulos, "Ultraviolet MSM photodetector based on GaN micromachining," *IEEE In Semiconductor Conference, 2008. CAS 2008. International,* vol. 1, pp. 91-94, 2008.

[6] R. D. L. IBM Corporation, "INTERDIGITATED SCHOTTKY BARRIER PHOTODETECTOR". United States of America Patent 4,772,931, 20 SEPTEMBER 1988.

[7] G. F. Camacho-Gonzalez, O. Olmos-Lopez, J. Sumaya-Martinez and M. Mayorga-Rojas, "Enhanced transmission through metallic subwavelength slits," *In Eighth Symposium Optics in Industry. Internation Society of Optics and Photonics,* vol. 8287, p. 82870T, 2011.

[8] X. Hu, M. Li, Z. Ye, W. Y. Leung, K.-M. Ho and S.-Y. Lin, "Design of midinfrared photodetectors enhanced by resonant cavities with subwavelength metallic gratings," *Applied Physics Letters,* vol. 93, 2008.

[9] R. A. Pala, J. S. Liu, E. S. Barnard, D. Askarov, E. C. Garnett, S. Fan and M. L. Brongersma, "Optimization of non-periodic plasmonic light-trapping layers for thin-film solar cells," *NATURE COMMUNICATIONS,* vol. 4, 2013.

[10] C.-C. Chang, Y. D. Sharma, Y.-S. Kim, J. A. Bur, R. V. Shenoi, S. Krishna, D. Huang and S.-Y. Lin, "A Surface Plasmon Enhanced Infrared Photodetector Based on InAs Quantum Dots," *NANO Letters,* vol. 10, no. 5, p. 1704–1709, 2010.

[11] S. Collin, F. Pardo and P. Jean-Luc, "Resonant-cavity-enhanced subwavelength metal–semiconductor–metal photodetector," *Applied Physics Letters,* vol. 83, 2003.

[12] K. Kishino, M. S. Ünlü, J.-I. Chyi, J. Reed, L. Arsenault and H. Morkoç, "Resonant Cavity-Enhanced (RCE) Photodetectors," *IEEE Journal of Quantum Electronics,* vol. 27, no. 8, pp. 2025-2034, 1991.

[13] J. B. Héroux, Y. X. and W. I. Wang, "GaInNAs resonant-cavity-enhanced photodetector operating at 1.3 mm," *Applied Physics Letters,* vol. 75, no. 18, pp. 2716-2718, 1999.

[14] A. Alù, G. D'Aguanno, N. Mattiucci and M. J. Bloemer, "Plasmonic Brewster Angle: Broadband Extraordinary Transmission through Optical Gratings," *Physical Review Letters,* vol. 106, no. 12, p. 123902, 2011.

[15] F. Xia, T. Mueller, Y. M. Lin, A. Valdes-Garcia and P. Avouris, "Ultrafast graphene photodetector," *Nature nanotechnology,* vol. 4, no. 12, pp. 839-843, 2009.

[16] T. Mueller, F. Xia and P. Avouris, "Graphene photodetectors for high-speed optical communications," *Nature Photonics,* vol. 4, no. 5, pp. 297-301, 2010.

[17] Z. Song, P. Wang, L. Guo, Y. Yang and Q. & Tang, "Asymmetric semicircular and triangular electrode structures to increase photo-to-dark-current ratio in MgZnO metal semiconductor metal photodetectors," *Japanese Journal of Applied Physics,* vol. 54, no. 5, p. 052201, 2015.

[18] P. G. Kik, "Catoptric electrodes: transparent metal electrodes using shaped surfaces," *Optics Letters,* vol. 39, no. 17, 1 September 2014.

[19] "LENA Lighting," 2010. [Online]. Available: http://www.lenalighting.pl/en/knowledge/spectrum-of-visible-radiation/.

[20] D. J. Wagner, "Glossary for Semiconductors," Rensselaer Polytechnic Institute, 2004. [Online]. Available: http://www.rpi.edu/dept/phys/ScIT/InformationProcessing/semicond/sc_glossary/scglossary.htm.

[21] "Indian Nanoelectronics User's Programme," INUP IISC BANGALORE, 2010. [Online]. Available: http://www.nano.iisc.ernet.in/inup/ghusoonali.html.

[22] Y. Cao, K. Cai, P. Hu, L. Zhao, T. Yan, W. Luo, X. Zhang, X. Wu, K. Wang and H. Zheng, "Strong enhancement of photoresponsivity with shrinking the electrodes spacing in few layer GaSe photodetectors," *scientific reports,* vol. 5, no. 8130, 2015.

[23] E. Hecht, Optics, San Francisc, CA: Adison Wesley, 2002.

[24] L. Novotny and B. Hecht, Principles of Nano-Optics, New York: Cambridge University Press, 2006.

[25] M. Born and E. Wolf, Principles of optics: electromagnetic theory of propagation, interference and diffraction of light, Cambridge Univesity Press, 1999.

[26] W. M. Haynes, Handbook of Chemistry and Physics, CRC, 2014-2015.

[27] [Online]. Available: https://code.google.com/p/lamp-solar/source/browse/trunk/data/optical_constants/?r=915#optical_constants. [Accessed 06 May 2015].

[28] P. N. J. Dennis, Photodetectors: An Introduction to Current Technology, New York: Plenum Press, 1987.

[29] S. Donati, "Photodetectors: Devices, Circuits and Applications," New Jersey, Prentice Hall, Inc., 2000.

[30] S. M. Sze and K. K. NG, "Physics of semiconductor devices," John Wiley & Sons, 2006, pp. 663-719.